

Effects of long-range taxis and population pressure on the range expansion of invasive species in heterogeneous environments

Kohkichi Kawasaki¹ · Nanako Shigesada² · Mamiko Iinuma³

Received: 14 October 2016 / Accepted: 10 January 2017 / Published online: 1 February 2017
© The Author(s) 2017. This article is published with open access at Springerlink.com

Abstract We consider a new model for biological invasions in periodic patchy environments, in which long-range taxis and population pressure are incorporated in the framework of reaction-diffusion-advection equations. We assume that long-range taxis is induced by a weighted integral of stimuli within a certain sensing range. Population pressure is incorporated in the diffusion coefficient that linearly increases with population density. We first analyze the model in the absence of population pressure and demonstrate how the sensing length of long-range taxis influences the range expansion pattern of invasive species and its rate of spread. The effects of population pressure are examined for both homogeneous and periodic patchy environments. For the homogeneous environment, an exact and explicit traveling wave solution and the spreading speed are obtained. For the periodic patchy environment, we find numerically that a population starting from any localized distribution evolves to a traveling periodic wave if the null solution of the RDA equation is locally unstable, and that the traveling wave speed significantly increases with increasing population pressure. Furthermore, the population pressure and

taxis intensity synergistically enhance the spreading speed when they are increased together.

Keywords Reaction-diffusion-advection · Periodic patchy environment · Traveling periodic wave · Long-range taxis · Population pressure

Introduction

The environments of living organisms are often fragmented by natural or artificial destruction of habitats. Invading organisms also expand their range in heterogeneous/fragmented landscapes. Whereas most theoretical studies on biological invasion have assumed that environments are homogeneous (Skellam 1951; for review, see Shigesada and Kawasaki 1997; Okubo and Levin 2001; Lewis et al. 2016), recent theoretical developments have increasingly been directed toward more realistic situations involving environmental heterogeneity, temporal variability, or interactions with other species (Chesson 2000; Hastings et al. 2005). Specifically, in the case of environments that change periodically in space, the spatio-temporal process of biological invasion has been investigated intensively in the framework of a reaction-diffusion equation (RDE model) or integro-difference equation (IDE model) to provide various new insights into the range expansion pattern and its spreading speed (RDE model: Shigesada et al. 1986; Weinberger 2002; Kinezaki et al. 2003, 2010; Berestycki et al. 2005a, b; Roques and Stoica 2007; IDE model: Kawasaki and Shigesada 2007; Lutscher 2008; Weinberger et al. 2008; Dewhurst and Lutscher 2009; Samia and Lutscher 2010; Gilbert et al. 2014; Musgrave and Lutscher 2014; Musgrave et al. 2015; Bengfort et al. 2016). More recently, increasing attention has been focused on the effects of directed movement

✉ Kohkichi Kawasaki
kkawasak@mail.doshisha.ac.jp

Nanako Shigesada
nshigesada@oak.dti.ne.jp

¹ Faculty of Culture and Science, Doshisha University,
Kyotanabe 610-0321, Japan

² Professor Emeritus of Nara Women's University,
13-49 Kawara Hirata, Kyotanabe 610-0361, Japan

³ Graduate School of Culture and Science, Doshisha University,
Kyotanabe 610-0321, Japan

toward more favorable habitats (taxis) on biological invasion (Mistro et al. 2005; Lutscher et al. 2006; Cantrell et al. 2006; Kawasaki et al. 2012; Vergni et al. 2012; Maciel and Lutscher 2013, 2015; Li et al. 2015; Shigesada et al. 2015).

Many organisms, from bacteria to mammals, have the ability to migrate in response to stimuli or signals that indicate food, favorable or unfavorable habitat, prey or predators, etc., through various senses such as sight, hearing, smell, touch and so on. Thus, these organisms are actively driven toward more favorable regions in heterogeneous environments. In the present study, we classify taxes into two major types, short-range taxis and long-range taxis, depending on the sensing range of the organisms. With respect to short-range taxis, we consider the case in which the sensing range is so narrow, i.e., close to or less than the body size, that organisms can only perceive the local intensity of the signal and/or its gradient (Shigesada et al. 2015). On the other hand, long-range taxis, as typically seen in higher animals, represents the case in which organisms can perceive environmental stimuli over a range wider than the body size, by means of sight and other appropriate senses, and move in the direction where a weighted integral of stimuli within their sensing range is larger.

A classical example of short-range taxis is chemotaxis, i.e., the movement of organisms in response to chemical gradients (Keller and Segel 1970; see also Hillen and Painter 2009). Such gradient-based taxis has been extended to higher animals in an ecological context (Shigesada et al. 1979; Shigesada and Roughgarden 1982; White et al. 1996; Turchin 1998; Okubo and Levin 2001; Cantrell et al. 2006). On the other hand, in small organisms such as bacteria, the body length is too short to measure gradients along the body axis. To resolve this problem, Othmer and Hillen (2002) presented a non-local model by using an integro-differential equation (see also Hillen and Painter 2009). However, this type of model is beyond the scope of the present work (but see the “Discussion” section).

Recently, Shigesada et al. (2015) studied a reaction-diffusion-advection equation with short-range taxis in periodic patchy environments in one dimension and investigated how short-range taxis and the patchy environment interplay to determine the spatio-temporal distribution of invasive species and its rate of spread (see also Maciel and Lutscher 2013). As a further step, the present study addresses a model that incorporates long-range taxis and compares its effects on the range-expansion of invasive species with those obtained from the corresponding short-range taxis model.

In the presence of taxis, either short-range or long-range, the population in the favorable patches should inevitably become overcrowded. However, it has been observed with various insects and animals that as the population density becomes higher, repulsive interferences among individuals

could induce density-dependent accelerated dispersal (Kono 1952; Watanabe et al. 1952; Myers and Krebs 1974; Okubo and Levin 2001). This effect is referred to as population pressure. Since Gurney and Nisbet (1975) first constructed density-dependent diffusion models, several authors have explored the density-dependent dispersal phenomenon from various angles (Gurtin and MacCamy 1977; Namba 1980; Shigesada 1980; Mimura and Kawasaki 1980; Sánchez-Garduño and Maini 1994; Lutscher 2008).

On the other hand, Morisita (1954) and Morisita (1971) quantitatively evaluated population pressure by counting the numbers of antlions that settled in a patchy environment which consisted of a favorable patch filled with fine sands and an unfavorable patch with coarse sands. The antlions showed a strong preference for fine sand over coarse sand for pit formation, when the population density was low. However, this tendency was gradually diminished with increasing densities, until almost equal numbers of individuals were settled in both sands. In order to quantitatively explain this result, he derived an empirical formula for the probability of settlement of an individual in each patch as a function of the total number of antlions initially released and the environmental favorabilities of the two patches. Based on Morisita’s experimental data, Shigesada et al. (1979) proposed a non-linear diffusion model for population pressure, in which the diffusion coefficient is given by a linearly increasing function of population density (see also Shigesada 1980). In the present study, we apply this non-linear diffusion term to the reaction-diffusion-advection equation for the periodic patchy environment and investigate how long-range taxis, population pressure, and environmental heterogeneity mutually influence in determining the rate of spread of invading species.

The layout of this article is as follows. In the “[Reaction-diffusion-advection equations incorporating active movement toward favorable environments](#)” section, the short- and long-range taxis functions are defined in the framework of a reaction-diffusion-advection equation for periodic environments in one dimension, and a brief summary of our previous related work is presented. In the “[Long-range taxis model in periodic patchy environments](#)” section, the reaction-diffusion-advection equation with long-range taxis for periodic patchy environments is mathematically analyzed to obtain the formula for the minimum speed of traveling waves. In the “[Effects of population pressure](#)” section, a non-linear reaction-diffusion-advection equation incorporating population pressure is introduced. First, we derive an exact traveling wave solution of this model for a special case when the environment is homogeneous, so that the effect of population pressure on the traveling wave speed is explicitly evaluated. Then, the asymptotic spreading speed of the same model for periodic patchy environments is numerically analyzed. In the “[Discussion](#)” section, we summarize the results

and discuss our findings in comparison with other relevant works.

Reaction-diffusion-advection equations incorporating active movement toward favorable environments

Short- and long-range taxis models

We consider a periodically varying environment with spatial period L in one dimension and investigate the invasion processes of a single species by employing the following reaction-diffusion-advection equation:

$$\frac{\partial n}{\partial t} = D \frac{\partial^2 n}{\partial x^2} - \frac{\partial u(x)n}{\partial x} + (r(x) - \mu n)n \text{ for } x \in (-\infty, \infty), \tag{1}$$

where n represents the population density $n(x, t)$ as a function of position x and time t . D , $u(x)$ and $(r(x) - \mu n)n$ are the diffusion coefficient, taxis velocity and growth function of the logistic type, respectively, where $u(x)$ and $r(x)$ are periodic functions of spatial period L , and D and μ are positive constants. The taxis velocity, $u(x)$, is supposed to change with species, depending on by what means and how far they sense the favorability of the environment. Here, we propose two kinds of advection velocities, short-range and long-range taxis velocities, as defined below.

(i) Taxis velocity caused by short-range taxis

Let $f(x)$ be the favorability of an environment at x for an organism. Here, we assume that the organism has a very narrow sensing range so that it can perceive the gradient of favorability only within its immediate vicinity. Thus, the taxis velocity at x is given by

$$u(x) = \alpha \frac{df(x)}{dx}, \tag{2}$$

where α is referred to as the sensitivity to gradient-based stimulus (Shigesada et al. 2015).

(ii) Taxis velocity caused by long-range taxis

For long-range taxis, we assume that an organism can survey and evaluate spatial changes in favorability on both right and left sides, and move toward the direction where a weighted integral of the stimuli is larger. More specifically, we denote by $F(x)$ the difference between the weighted integrals of favorabilities on the right and left sides as follows (Kawasaki 1978; Turchin 1998):

$$F(x) = \int_0^\infty s(\xi) f(\xi + x) d\xi - \int_{-\infty}^0 s(\xi) f(\xi + x) d\xi, \tag{3a}$$

where $s(\xi)$ represents the sensory acuity for objects at distance ξ from the organism, which satisfies

$$s(\xi) = s(-\xi) \geq 0 \text{ and } \frac{ds(\xi)}{d\xi} < 0 \text{ for } \xi > 0, \tag{3b}$$

$$\text{and } \int_0^\infty s(\xi) d\xi = m,$$

where m is a positive constant. $F(x)$ is hereafter referred to as the integral-based stimulus. We further assume that the integral-based stimulus would be processed through the organism’s nervous and locomotive systems to induce taxis with velocity $u(x)$ that is generally given in the following form:

$$u(x) = G(F(x)), \tag{4a}$$

where $G(y)$ with y substituting for $F(x)$ satisfies

$$\frac{dG(y)}{dy} \geq 0, G(y) = -G(-y), \text{ and } \lim_{y \rightarrow \pm\infty} G(y) = \pm \hat{u}. \tag{4b}$$

The first inequality means that the taxis velocity increases with increase in the integral-based stimulus, y . The second equation indicates that $G(y)$ is odd with respect to $y = 0$ (i.e., the magnitudes of the taxis velocity are the same for integral-based stimuli, y and $-y$, although their directions are opposite). In the last equation, \hat{u} represents the maximum taxis speed physiologically attainable for the organism and is referred to as the taxis intensity. For example, the following function satisfies the above conditions (White et al. 1996; Okubo and Levin 2001)

$$G(y) = \hat{u} \tanh(\theta y), \tag{5}$$

where $\theta (> 0)$ is referred to as the sensitivity to integral-based stimulus. Particularly, when θ is very large, $G(y)$ is approximated by

$$G(y) = \hat{u} \operatorname{sgn}(y), \tag{6}$$

where $\operatorname{sgn}(y) = 1$ for $y > 0$, 0 for $y = 0$ and -1 for $y < 0$.

Previous work — existence of asymptotic spreading speeds and traveling periodic waves

Recently, Shigesada et al. (2015) investigated the following general class of reaction-diffusion-advection equations to address the large-time asymptotics of a solution and its spreading speed:

$$\frac{\partial n}{\partial t} = \frac{\partial}{\partial x} \left(D(x) \frac{\partial n}{\partial x} \right) - \frac{\partial u(x)n}{\partial x} + R(x, n)n \text{ in } x \in (-\infty, \infty), \tag{7}$$

where $D(x)$, $u(x)$, and $R(x, n)$ are periodic functions of L in x . They presented a theorem about the existence of

asymptotic spreading speeds and periodic traveling waves, and the relations between the asymptotic spreading speeds and the speeds of certain traveling wave solutions (see Theorem 2.1 of Shigesada et al. (2015)). Since (1) is a special case of Eq. 7 in which $D(x)$ and $R(x, n)$ are substituted by constant D and the per capita logistic growth rate, $r(x) - \mu n$, respectively, the theorem for the general class of reaction-diffusion-advection Eq. 7 is simplified for Eq. 1 as follows:

Theorem 1 *Let the prescribed functions in Eq. 1 satisfy the following properties: (i) $r(x)$ is uniformly bounded, (ii) $u(x)$ is integrable, uniformly bounded and piecewise continuous, and (iii) the equilibrium solution $n = 0$ of Eq. 1 is unstable. Then, the following statements hold.*

- I. *Existence of traveling periodic waves: There exist traveling periodic wave solutions (TPWs) to the left and right. A rightward TPW of speed c is defined as follows:*

$$n(x, t - L/c) = n(x + L, t) \text{ for any } x \text{ and } t, \tag{8}$$

$$\lim_{x \rightarrow \infty} n(x, t) = 0, \quad \lim_{x \rightarrow -\infty} (n(x, t) - n^*(x)) = 0,$$

where $n^*(x)$ is a uniformly positive L -periodic equilibrium solution of Eq. 1. Equation 8 means that the spatial pattern of the TPW at any t shifts forward by one spatial period L with the lapse of time interval $\tau = L/c$. The leftward TPW is defined in a similar way.

- II. *Existence of asymptotic spreading speeds: There exist two numbers c_-^* and c_+^* with $-c_-^* \leq c_+^*$ such that every solution $n(x, t)$ of Eq. 1 with $0 \leq n(x, 0) < n^*(x)$, $n(x, 0) > 0$ on an open interval, and $n(x, 0) = 0$ outside a bounded set propagates to the right and left, and has the following properties:*

$$\begin{aligned} \lim_{t \rightarrow \infty} \max_{x \leq -ct} n(x, t) &= 0 \text{ when } -c < -c_-^*, \\ \lim_{t \rightarrow \infty} \max_{-c-t \leq x \leq ct} (n^*(x) - n(x, t)) &= 0 \\ &\text{when } -c_-^* < -c_- < c_+ < c_+^*, \\ \lim_{t \rightarrow \infty} \max_{x \geq ct} n(x, t) &= 0 \text{ when } c > c_+^*. \end{aligned} \tag{9}$$

That is, c_+^* and c_-^* are the rightward and leftward asymptotic spreading speeds, respectively.

- III. *Relation between asymptotic spreading speeds and TPW speeds: The rightward asymptotic spreading speed c_+^* can be characterized as the smallest c for which a rightward TPW of speed c exists. Also c_-^* is the smallest speed of a leftward TPW of Eq. 1.*
- IV. *Relation between asymptotic spreading speeds and certain TPW speeds of the linearized equation of Eq. 1: c_+^* can be characterized as the smallest speed c*

for which the linearization

$$\frac{\partial n}{\partial t} = D \frac{\partial^2 n}{\partial x^2} - \frac{\partial u(x)n}{\partial x} + r(x)n, \tag{10a}$$

of (1) has a solution of the form,

$$n(x, t) = e^{-s(x-ct)} g(x), \tag{10b}$$

with $s > 0$ and $g(x)$ being L -periodic (see also Shigesada et al. 1986; Weinberger 2002; Berestycki et al. 2005b).

By using Theorem 1, we have already examined (1) for periodic environments in which favorable and unfavorable patches are alternately arranged in one dimension and the taxis velocity $u(x)$ is caused by the short-range taxis as given by Eq. 2 with the favorability $f(x)$ proportional to $r(x)$ (Shigesada et al. 2015). Solving its linearized equation as given by Eq. 10, we obtained the formula for the asymptotic speed c^* as a function of parameters involved in Eq. 1.

In the next section, we again deal with Eq. 1 in the same periodic patchy environments as described above except that the taxis velocity is given by the long-range taxis model defined in the “Short- and long-range taxis models” section (ii).

Long-range taxis model in periodic patchy environments

Taxis velocity

Consider (1) in a periodic patchy environment with favorable and unfavorable patches alternately arranged. Here, we assume that $r(x)$ is a piecewise constant function as follows (Shigesada et al. 1986; Shigesada et al. 2015):

$$r(x) = \begin{cases} r_1 & (x_{2m} \leq x < x_{2m+1}) \\ r_2 & (x_{2m+1} \leq x < x_{2m+2}) \end{cases} \tag{11}$$

$$x_{2m} = mL, \quad x_{2m+1} = mL + l_1 \quad \text{and} \quad L = l_1 + l_2 \quad (m = 0, \pm 1, \pm 2, \dots),$$

where l_1 and l_2 are the widths of the favorable and unfavorable patches, respectively; and x_{2m} and x_{2m+1} indicate the left and right boundaries of the favorable patch located between $x = mL$ and $mL + l_1$. The intrinsic growth rate $r(x)$ is set to $r_1 (> 0)$ and $r_2 (< r_1)$ in the favorable and unfavorable patches, respectively.

As for the taxis velocity $u(x)$, we need to fix explicit forms of the three functions, $f(x)$, $s(x)$, and $G(y)$ defined in the “Short- and long-range taxis models” section (ii). As

a simple and mathematically tractable candidate, here, we adopt the following functions:

$$f(x) = r(x), \tag{12a}$$

$$s(\xi) = s(-\xi) > 0 \text{ for } |\xi| < \sigma, \quad s(\xi) = 0 \text{ for } |\xi| \geq \sigma$$

$$\text{and } \frac{ds(\xi)}{d\xi} < 0 \text{ for } 0 < \xi < \sigma, \tag{12b}$$

$$G(y) = \hat{u} \operatorname{sgn}(y). \tag{12c}$$

In Eq. 12a, $r(x)$ is chosen for the favorability of the environment at x (Shigesada and Roughgarden 1982; Cantrell et al. 2006). In Eq. 12b, conditions of $s(\xi) > 0$ for $|\xi| < \sigma$ and $s(\xi) = 0$ for $|\xi| \geq \sigma$ are additionally imposed on the sensory acuity defined in Eq. 3b, because any organism generally has a limit to its sensory ability. Hereafter, σ is referred to as sensing length. For $G(y)$, we adopt (6) for simplicity so that an organism undergoes taxis to the right or left at the maximum speed \hat{u} as long as the integral-based stimulus y is not zero, and there is no taxis where $y = 0$ (but see the “More generalized models” section for $G(y)$ in a more general case).

Now applying (12) to (1) and rewriting $u(x)$ and $F(x)$ to $u_\sigma(x)$ and $F_\sigma(x)$, respectively, we have a long-range taxis model with the sensing length σ in the framework of a reaction-diffusion-advection equation,

$$\frac{\partial n}{\partial t} = D \frac{\partial^2 n}{\partial x^2} - \frac{\partial u_\sigma(x)n}{\partial x} + (r(x) - \mu n)n, \tag{13a}$$

where

$$u_\sigma(x) = \hat{u} \operatorname{sgn}(F_\sigma(x)), \tag{13b}$$

$$F_\sigma(x) = \int_0^\sigma s(\xi)r(\xi+x)d\xi - \int_{-\sigma}^0 s(\xi)r(\xi+x)d\xi. \tag{13c}$$

Since $r(x)$ is L -periodic in x (i.e., $r(x) = r(x + L)$) and even with respect to $x = l_1/2$ (i.e., $r(x) = r(l_1 - x)$) and $s(\xi)$ is even with respect to $\xi = 0$, $F_\sigma(x)$ has the following general properties for any given $\sigma > 0$ (see Appendix A for proof):

$$F_\sigma(x) = F_\sigma(x + L) \quad (L\text{-periodic in } x), \tag{14a}$$

$$F_\sigma(x) = -F_\sigma(l_1 - x) \quad (\text{odd with respect to } x = l_1/2). \tag{14b}$$

Applying the above equations to Eq. 13b, we have

$$u_\sigma(x) = u_\sigma(x + L) \quad (L\text{-periodic in } x), \tag{15a}$$

$$u_\sigma(x) = -u_\sigma(l_1 - x) \quad (\text{odd with respect to } x = l_1/2). \tag{15b}$$

Thus, we focus on the region $0 \leq x < L$ and calculate (13c) to have $u_\sigma(x)$ for $\sigma > 0$ as follows (see Appendix B for proof):

$$u_\sigma(x) = \begin{cases} \hat{u} & (0 \leq x < \sigma_1) \\ 0 & (\sigma_1 \leq x \leq l_1 - \sigma_1) \\ -\hat{u} & (l_1 - \sigma_1 < x < l_1 + \sigma_2) \\ 0 & (l_1 + \sigma_2 \leq x \leq L - \sigma_2) \\ \hat{u} & (L - \sigma_2 < x \leq L) \end{cases} \tag{16}$$

where $\sigma_1 = \min(\sigma, l_1/2)$ and $\sigma_2 = \min(\sigma, l_2/2)$.

Figure 1 illustrates $u_\sigma(x)$ and $r(x)$ when $l_1 \geq l_2$ by the solid and dashed lines, respectively. In Fig. 1a, where the organism has a sensing length σ such that $0 \leq \sigma < l_2/2$, there are six subintervals in one spatial period, $(0, \sigma)$, $(\sigma, l_1 - \sigma)$, $(l_1 - \sigma, l_1)$, $(l_1, l_1 + \sigma)$, $(l_1 + \sigma, L - \sigma)$, and $(L - \sigma, L)$. In each subinterval, both $r(x)$ and $u_\sigma(x)$ are constant, whereas at the interfaces between adjacent subintervals, either $r(x)$ or $u_\sigma(x)$ is discontinuous. When the organism is located within σ from the nearest interface, it undergoes taxis with velocity \hat{u} or $-\hat{u}$, because the weighted integral of favorability differs between the left and right sensing ranges. However, when the organism is located away from the interface by more than σ but less than $l_2/2$, its taxis velocity becomes zero, because the weighted integral of favorability is the same on both sides. In Fig. 1b, in which the organism has a sensing length σ such that $l_2/2 \leq \sigma < l_1/2$, there remains no subinterval where $u_\sigma(x) = 0$ within the unfavorable

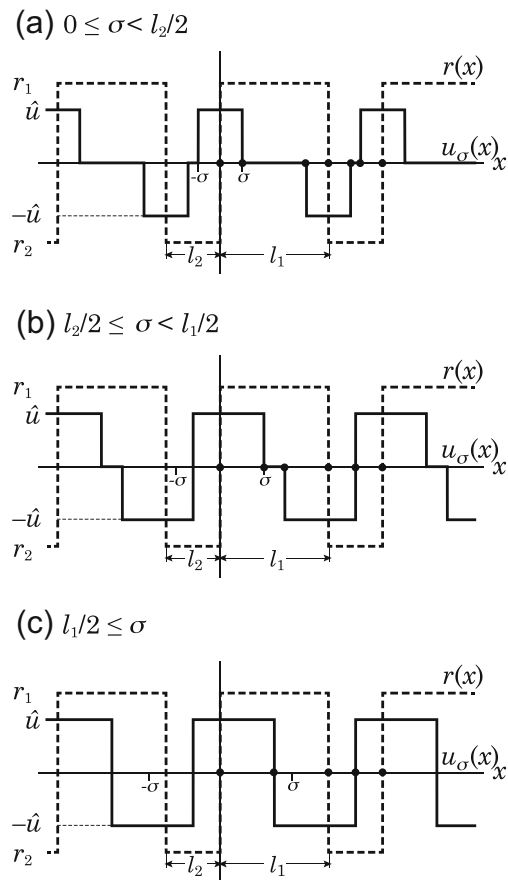


Fig. 1 Taxis velocity function $u_\sigma(x)$ of the long-range taxis when $l_2 \leq l_1$. The solid and dashed lines indicate $u_\sigma(x)$ and the intrinsic growth rate, $r(x)$, respectively. Depending on the sensing length, σ , $u_\sigma(x)$ shows three different patterns that consist of 6, 5, and 4 subintervals in one spatial period ranging $0 \leq x < L$, when **a** $0 \leq \sigma < l_2/2$, **b** $l_2/2 \leq \sigma < l_1/2$, and **c** $l_1/2 \leq \sigma$, respectively. In all cases, $u_\sigma(x)$ is L -periodic in x and even with respect to $x = l_1/2$

patch. Thus, the number of the subintervals is reduced to five. Furthermore, in Fig. 1c for which $\sigma \geq l_1/2$, there is no subinterval where $u_\sigma(x) = 0$ in either the favorable patch or the unfavorable patch except for the points at $x = l_1/2$ and $x = l_1 + l_2/2$, so that the number of subintervals becomes four. This means that organisms located in the areas between the centers of unfavorable patches and their respective right adjacent favorable patch move toward the right at speed \hat{u} , whereas those located in the remaining areas move toward the left at the same speed.

On the other hand, when $l_1 < l_2$, three types of patterns of $u_\sigma(x)$ that are similar to those in Fig. 1 appear, though the figure corresponding to Fig. 1b contains no subinterval where $u_\sigma(x) = 0$ within the favorable patch, rather than the unfavorable patch. Overall, as the sensing length σ increases from 0, the area where the taxis occurs enlarges until it covers the whole space when σ reaches $\max(l_1/2, l_2/2)$ and stays constant thereafter.

It should be noted that when $l_1 = l_2 = L/2$, the pattern in Fig. 1b disappears. Incidentally Kawasaki et al. (2012) previously studied, a similar problem for a specific case of $l_1 = l_2 = L/2, \sigma = L/4, s(\xi) = 1$ for $|\xi| < \sigma$ and $s(\xi) = 0$ for $|\xi| \geq \sigma$.

Asymptotic spreading speed of Eq. 13

Since both $r(x)$ and $u_\sigma(x)$ in Eq. 13 are piecewise constant and L -periodic as seen in Fig. 1, assumptions (i) and (ii) in Theorem 1 are satisfied. Therefore, if assumption (iii) is satisfied, i.e., the equilibrium solution $n = 0$ of Eq. 13 is unstable, all the statements (I)–(IV) of Theorem 1 in the “Previous work — existence of asymptotic spreading speeds and traveling periodic waves” section hold. Hereafter, under the condition that $n = 0$ is unstable, we use statement (III) to estimate the rightward asymptotic spreading speed c^* by the minimum speed of TPWs of Eq. 13, which will be designated the minimum TPW speed c^* hereafter. To be noted, from statements (III) and (IV) of Theorem 1, the minimum TPW speed c^* equals the minimum speed of solutions of the linearized Eq. 10a in the form of Eq. 10b. The leftward asymptotic spreading speed is evidently the same as the rightward spreading speed, because $r(x)$ is L -periodic in x and even with respect to $x = l_1/2$.

Consider the linearized equation of (13) about $n = 0$,

$$\frac{\partial n}{\partial t} = D \frac{\partial^2 n}{\partial x^2} - \frac{\partial u_\sigma(x)n}{\partial x} + r(x)n, \tag{17}$$

and a solution of Eq. 17 having the following form:

$$n(x, t) = e^{-sz}g(x), \tag{18}$$

where $z = x - ct, g(x) = g(x + L)$ and $s > 0$.

Since the right-hand side of (18) can be factored into a product of functions of t and x , we set $p(x) = e^{-sx}g(x)$,

substitute $n(x, t) = e^{cst}p(x)$ in Eq. 17 and further put $q(x) = Dp' - u_\sigma(x)p$. Then, Eq. 17 becomes a system of first order differential equations,

$$\begin{pmatrix} p' \\ q' \end{pmatrix} = \begin{pmatrix} u_\sigma(x)/D & 1/D \\ cs - r(x) & 0 \end{pmatrix} \begin{pmatrix} p \\ q \end{pmatrix}. \tag{19}$$

On the other hand, since $u_\sigma(x)$ and $r(x)$ are L -periodic, the condition that $g(x)$ is L -periodic is rewritten in terms of p and q as

$$\begin{pmatrix} p(x + L) \\ q(x + L) \end{pmatrix} = e^{-sL} \begin{pmatrix} p(x) \\ q(x) \end{pmatrix}. \tag{20}$$

Thus, we only need to solve (19) with (20) for one spatial period. Here, we focus on the interval, $(0, L)$. As shown in Fig. 1, one interval contains six, five, or four subintervals, depending on the sensing length, σ . Since all the coefficients in Eq. 19 are uniformly bounded and piecewise constant, there exists a solution of (19) that is continuous across each boundary between subintervals:

$$p(x_i^+) = p(x_i^-), \tag{21a}$$

$$q(x_i^+) = q(x_i^-), \tag{21b}$$

where x_i is the location of an interface between two adjacent subintervals. Since $n(x, t) = e^{cst}p(x)$ and $-D\partial n/\partial x + u_\sigma(x)n = -e^{cst}q(x)$, Eqs. 21a and 21b correspond to continuity conditions of the population density and the flux at the interface, respectively. As these conditions are biologically reasonable and feasible, we adopt conditions (21) in the following analyses.

We first solve (19) on $(0, L)$ for the case of $0 \leq \sigma \leq l_2/2$ that involves six subintervals, $(0, \sigma_1), (\sigma_1, l_1 - \sigma_1), (l_1 - \sigma_1, l_1), (l_1, l_1 + \sigma_2), (l_1 + \sigma_2, L - \sigma_2)$, and $(L - \sigma_2, L)$ (see Fig. 1a). Since $r(x)$ and $u_\sigma(x)$ are constant in each subinterval, we can easily solve (19) for each subinterval. Combining the resultant solutions with Eq. 21 successively, we have

$$\begin{pmatrix} p(L) \\ q(L) \end{pmatrix} = A^{(0,L)} \begin{pmatrix} p(0) \\ q(0) \end{pmatrix}, \tag{22a}$$

where

$$A^{(0,L)} = A_{(\hat{u}, r_2)}^{(L-\sigma_2, L)} A_{(0, r_2)}^{(l_1+\sigma_2, L-\sigma_2)} A_{(-\hat{u}, r_2)}^{(l_1, l_1+\sigma_2)} \times A_{(-\hat{u}, r_1)}^{(l_1-\sigma_1, l_1)} A_{(0, r_1)}^{(\sigma_1, l_1-\sigma_1)} A_{(\hat{u}, r_1)}^{(0, \sigma_1)}, \tag{22b}$$

$$A_{(u,r)}^{(a,b)} = e^{\frac{u(b-a)}{2D}} \times \begin{pmatrix} \cosh w + \frac{u}{2Dv} \sinh w & \frac{1}{Dv} \sinh w \\ \frac{\lambda - r}{v} \sinh w & \cosh w - \frac{u}{2Dv} \sinh w \end{pmatrix}, \tag{22c}$$

$$w = v(b - a), \quad v = \sqrt{\frac{\lambda - r}{D} + \frac{u^2}{4D^2}} \quad \text{and} \quad \lambda = cs.$$

Substituting (20) for $x = 0$ into (22a), we have the dispersion relation between c and s as follows:

$$\det \left(A^{(0,L)} - e^{-sL} I \right) = 0. \tag{23}$$

When there is a set of $c > 0$ and $s > 0$ that satisfies (23), the smallest c should be the asymptotic spreading speed c^* of Eq. 13 (cf. Theorem 1 IV). It should be noted that for the case of $l_2/2 \leq \sigma \leq l_1/2$ corresponding to Fig. 1b, $A_{(0,r_2)}^{(l_1+\sigma_2, L-\sigma_2)} = I$ holds because $\sigma_2 = \min(\sigma, l_2/2) = l_2/2$, and for the case of $\sigma \geq l_1/2$ corresponding to Fig. 1c, $A_{(0,r_1)}^{(\sigma_1, l_1-\sigma_1)} = I$ further holds because $\sigma_1 = \min(\sigma, l_1/2) = l_1/2$. Therefore, Eqs. 22 and 23 are valid for all these three cases.

Here, we briefly explain how to derive $c^* = \min c(s)$ from the dispersion relation. Since e^{-sL} is the eigenvalue of $A^{(0,L)}$ in which c and s are included only as $\lambda = cs$, the dispersion relation (23) can be rewritten in the form (see Appendix C):

$$s = \frac{1}{L} \cosh^{-1} \frac{\text{tr} A^{(0,L)}}{2} \equiv Q(\lambda), \tag{24}$$

where the positive branch of \cosh^{-1} is taken. Substituting (24) into $c = \lambda/s$ yields $c = \lambda/Q(\lambda)$. Thus, the minimum TPW speed of Eq. 13 is given as

$$c^* = \min_{\lambda > 0} \frac{\lambda}{Q(\lambda)}. \tag{25}$$

The criterion for successful invasion, i.e., the condition for the equilibrium $n = 0$ of Eq. 13 to be unstable, is given by $\text{tr} A^{(0,L)}|_{\lambda=0} < 2$ (see Appendix C.2).

Numerical results

We first numerically examine what spatio-temporal pattern the solution of Eq. 13 exhibits for a sufficiently large time. Numerical simulations are done for varying parameter values with initial distributions localized around the origin. We confirm that populations eventually go to extinction or evolve to a unique asymptotic wave that fits well with the TPW defined by Eq. 8 in Theorem 1, depending on whether the equilibrium $n = 0$ of Eq. 13 is stable or not (i.e., $\text{tr} A^{(0,L)}|_{\lambda=0} > 2$ or $\text{tr} A^{(0,L)}|_{\lambda=0} < 2$). We also calculate the minimum TPW speed c^* , from Eq. 25. These results are shown in Figs. 2 and 3, in which the three major parameters relevant to taxis, \hat{u} , σ , and r_2 , are varied, while the other parameters are fixed as $l_1 = 1$, $l_2 = 0.5$, and $D = r_1 = \mu = 1$. Note that we can set $D = r_1 = \mu = 1$ without loss of generality, if we non-dimensionalize (13) by putting $\mu n/r_1 \rightarrow N$, $r_1 t \rightarrow T$, and $\sqrt{r_1/D} x \rightarrow X$ (Kawasaki et al. 2012; Shigesada et al. 2015).

Panels (I), (II), and (III) in Fig. 2a illustrate asymptotic solutions numerically calculated for $\sigma = 0.1, 0.3$, and 0.5 , respectively, that fall within the ranges specified in Fig. 1a,

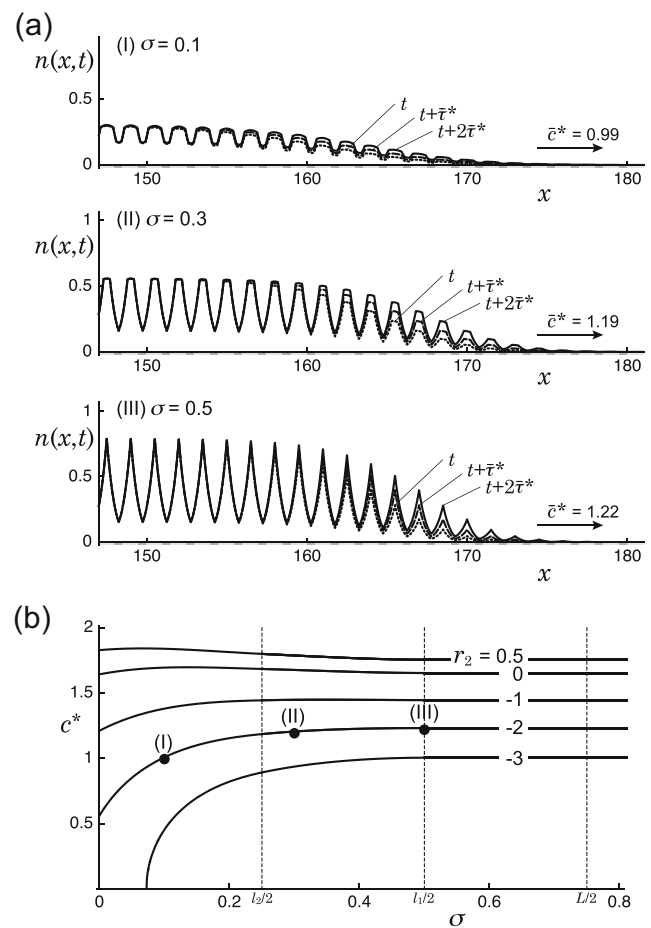


Fig. 2 Effects of the sensing length σ on the pattern and speed of large-time asymptotic solutions of the long-range taxis model. **a** The asymptotic solutions numerically obtained for (I) $\sigma = 0.1$, (II) $\sigma = 0.3$, and (III) $\sigma = 0.5$, taken at time interval $\bar{\tau}^*$, are plotted. The other parameters are $D = 1$, $\hat{u} = 2$, $r_1 = 1$, $r_2 = -2$, $l_1 = 1$, $l_2 = 0.5$, and $\mu = 1$. The asymptotic solutions closely satisfy the conditions for the TPW solutions defined by (8), where the values of t , $\bar{\tau}^*$ and \bar{c}^* are (I) 177.0, 1.49, and 0.99; (II) 148.1, 1.24, and 1.19; and (III) 143.7, 1.22, and 1.22, respectively. **b** The *solid lines* indicate the minimum TPW speed c^* obtained from Eq. 25 as a function of σ for $r_2 = -3, -2, -1, 0$, and 0.5 . The other parameters are the same as in **a**. When σ exceeds $l_1/2$, the speed c^* is kept constant at the same value as at $\sigma = l_1/2$. The *black circles* labeled (I), (II), and (III) correspond to the speeds \bar{c}^* numerically obtained in (I), (II), and (III) in **a**, respectively

b, c. The values of r_2 and \hat{u} are chosen as -2 and 2 , respectively. In each panel, three successive solutions taken at a given interval $\bar{\tau}^*$ (the overline signifies the value numerically obtained) are illustrated. Since these three patterns can be almost perfectly superimposed when one of them is moved toward the other by a spatial period L , these asymptotic solutions are supposed to have closely attained a TPW. Thus, we numerically estimate the TPW speed by $\bar{c}^* = L/\bar{\tau}^*$ (see Fig. 2a). As for the spatial patterns of the asymptotic solutions for any fixed t , population density n sharply increases or decreases with x where $u_\sigma(x) > 0$ or $u_\sigma(x) < 0$, respectively, whereas it changes only gently

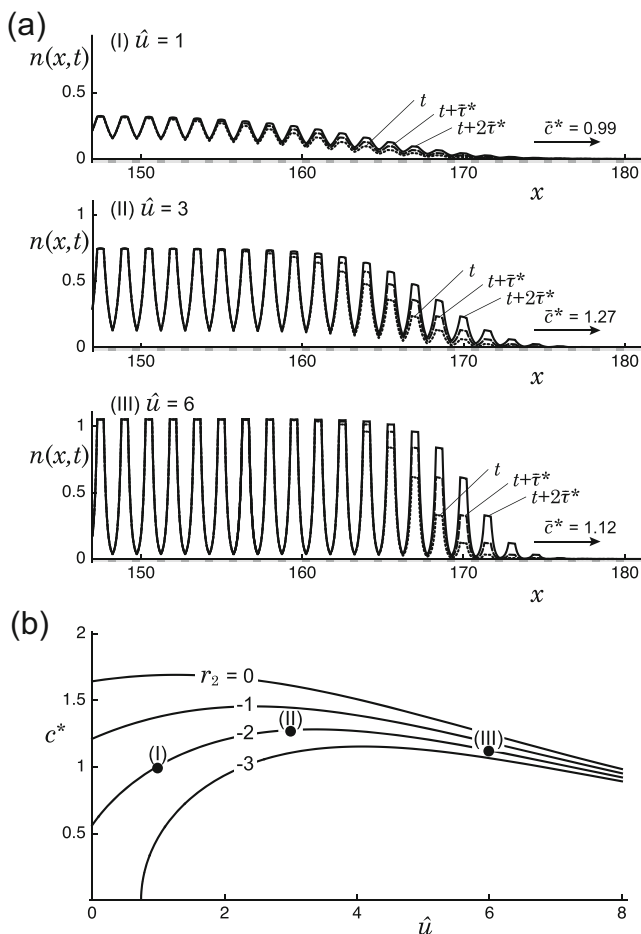


Fig. 3 Effects of the taxis intensity \hat{u} on the pattern and speed of asymptotic solutions of the long-range taxis model. **a** Asymptotic solutions numerically obtained when (I) $\hat{u} = 1$, (II) $\hat{u} = 3$, and (III) $\hat{u} = 6$, taken at time interval $\bar{\tau}^*$, are plotted. In all cases, σ is chosen as 0.3 and the other parameters are the same as in Fig. 2a. The asymptotic solutions closely satisfy the conditions for the TPW defined by Eq. 8, where the values of t , $\bar{\tau}^*$ and \bar{c}^* are (I) 177.1, 1.49, and 0.99; (II) 138.5, 1.17, and 1.27; and (III) 156.1, 1.33, and 1.12, respectively. **b** The solid lines indicate the minimum TPW speed c^* obtained from Eq. 25 as a function of \hat{u} for $r_2 = -3, -2, -1$, and 0. The other parameters are the same as in **a**. The black circles labeled (I), (II), and (III) correspond to the speed \bar{c}^* numerically obtained in (I), (II), and (III) in **a**, respectively

where $u_\sigma(x) = 0$. Particularly, when $\sigma = 0.5$ (i.e., case (III) in Fig. 2a), there is no place at which $u_\sigma(x) = 0$ so that organisms located within $\pm L/2$ of the center of the favorable patch are all attracted toward that center, resulting in a highly pointed distribution in the middle of each favorable patch.

In Fig. 2b, the minimum TPW speed c^* analytically obtained from Eq. 25 is shown by solid lines as a function of σ for varying values of r_2 . The speeds c^* for $r_2 = 0$ and 0.5 show slightly one-humped curves within the range $0 \leq \sigma \leq l_1/2$ and then stay constant for $\sigma \geq l_1/2$. This is explained as follows. The initial increase in the speed is brought about

because a moderate long-range taxis induces an accumulated distribution of organisms in the favorable patches, by which the overall growth rate is enhanced to result in accelerated speed. As σ increases further up to $l_1/2$, however, the speed tends to gradually decrease because excessive taxis to favorable patches hinders the dispersal of organisms through the adjacent unfavorable patches, thereby cancelling out the effect of the increased overall growth rate. Once σ exceeds $l_1/2$, the speed becomes constant, because the pattern of $u_\sigma(x)$ no longer depends on σ (see Fig. 1c). When $r_2 = -1$ or -2 , the speed initially shows rapid increases for the range $0 \leq \sigma \leq l_2/2$ ($= 0.25$) (Fig. 1a), but the rate of increase gradually diminishes for $l_2/2 \leq \sigma \leq l_1/2$ ($= 0.5$) (Fig. 1b), and then becomes zero when σ exceeds $l_1/2$ (Fig. 1c). When r_2 is further reduced to -3 , the speed c^* becomes zero for $0 < \sigma < 0.722$, because the equilibrium state $n = 0$ of Eq. 13 is stable (i.e., $\text{tr}A^{(0,L)}|_{\lambda=0} > 2$), and then abruptly shows a sharp rise followed by a saturating curve that becomes constant after $\sigma > l_1/2$. Black circles labeled (I), (II), and (III) represent the asymptotic speeds \bar{c}^* numerically obtained in (I), (II), and (III) of Fig. 2a, respectively, which closely fit the minimum TPW speed c^* as indicated by the solid curve for $r_2 = -2$.

We next examine the effects of the taxis intensity \hat{u} . Figure 3a illustrates the asymptotic solutions for $\hat{u} = 1, 3$, and 6 with the other parameters fixed as $\sigma = 0.3$ and $r_2 = -2$ (i.e., the pattern of $u_\sigma(x)$ is fixed to the case shown in Fig. 1b). We again confirm that those solutions have closely attained TPWs. As \hat{u} increases, the amplitude of the population density between favorable and unfavorable patches markedly increases, while the population density in the central region of the favorable patch where $u_\sigma(x) = 0$ remains almost flat. Particularly, when $\hat{u} = 6$, the population density is highly elevated in the favorable patches, whereas it is extremely reduced in the unfavorable patches. We also numerically estimate the asymptotic speed, $\bar{c}^* = L/\bar{\tau}^*$, to be 0.99, 1.27, and 1.12 for $\hat{u} = 1, 3$, and 6, respectively. Figure 3b shows the minimum TPW speed c^* obtained from Eq. 25 as a function of \hat{u} for $r_2 = 0, -1, -2$, and -3 . Closed circles labeled (I), (II), and (III) represent the speeds indicated in (I), (II), and (III) of Fig. 3a, respectively. For any value of r_2 , c^* exhibits a one-humped curve and tends to zero as $\hat{u} \rightarrow \infty$, because we have $c^* = O(1/\hat{u})$ as $\hat{u} \rightarrow \infty$ in Eq. 25. Comparing (a) and (b) in Fig. 3 suggests that the reduction in speed c^* at a large \hat{u} could be associated with extremely low population densities in the unfavorable patch as seen in Fig. 3a (III).

To summarize, although both the sensing length σ and the taxis intensity \hat{u} involved in long-range taxis are critical in controlling the minimum speed c^* , their effects essentially differ in that the speed c^* with respect to σ shows either monotonic or one-humped curves that become constant for $\sigma > \max(l_1/2, l_2/2)$, whereas the speed c^* with

respect to \hat{u} always shows one-humped curves that tend to zero at $\hat{u} \rightarrow \infty$.

More generalized models

In the “Short- and long-range taxis models” section (ii), we have presented a general taxis velocity function, $u(x) = G(F(x))$ where $F(x)$ and $G(y)$ are defined by Eqs. 3 and 4, respectively. Actually, we have focused on Eq. 13 only with the simplest taxis function $u(x)$ in which $r(x)$, $s(\xi)$, and $G(y)$ are given by Eqs. 11, 12b and 12c, respectively.

However, we can extend $r(x)$ somewhat to a more general function while maintaining L -periodicity in x and evenness with respect to $x = l_1/2$. In this case, Eqs. 14 and 15 still hold. Particularly, when $dr(x)/dx > 0$ for $-l_2/2 < x < l_1/2$, $u_\sigma(x)$ is given by Eq. 16 in the case of $\sigma_1 = l_1/2$ and $\sigma_2 = l_2/2$, which corresponds to Fig. 1c. However, if there exists a range of width d in which $r(x)$ is constant, we can predict that when $\sigma < d/2$, an area of length $d - 2\sigma$ where $u_\sigma(x) = 0$ appears in the middle of that range. Based on these considerations, when $G(y)$ is given by Eq. 12c, a method similar to that used in the “Asymptotic spreading speed of Eq. 13” section can be applied to obtain the TPW speed.

When $G(y)$ is given by a more generalized function such as Eq. 5, the mathematical formula for the minimum TPW speed, Eq. 25, is no longer available, because it is generally difficult to find an explicit solution of Eq. 19. Thus, intensive numerical simulations become necessary to derive TPW speeds c^* . Here, we present some numerical results for the case that $r(x)$ is given by Eq. 11, $s(\xi) = 2(1 - |\xi|/\sigma)/\sigma$ for $0 \leq |\xi| < \sigma$ and 0 for $|\xi| \geq \sigma$, and $G(y)$ is given by Eq. 5. Figure 4a shows $F_\sigma(x)$ (thick dashed curve) and $u_\sigma(x)$ (thin solid curves) for $\sigma = 0.4$ and $\theta = 1/2, 1, 2$, and 10 with the other parameters kept the same as in Fig. 2. As θ increases, $u_\sigma(x)$ monotonically changes to attain a step-wise function at $\theta = \infty$, namely, $u_\sigma = \hat{u} \operatorname{sgn}(F_\sigma(x))$. By using $u_\sigma(x)$ thus obtained for various σ and θ , we perform numerical simulations of Eq. 13. In Fig. 4b, the asymptotic speeds are plotted for $\theta = 1/2, 1, 2$, and 10 on to the same graph as Fig. 2b. As θ increases, the speed for each r_2 becomes closer to the corresponding solid line that represents the speed for $\theta \rightarrow \infty$. From this figure, we can see that the speed dependency on σ is qualitatively conserved for a wide range of θ .

Effects of population pressure

So far, we have investigated the long-range taxis model for patchy environments, Eq. 13, in which both the diffusion coefficient and the taxis velocity are assumed to be density independent and found that as the taxis intensity increases,

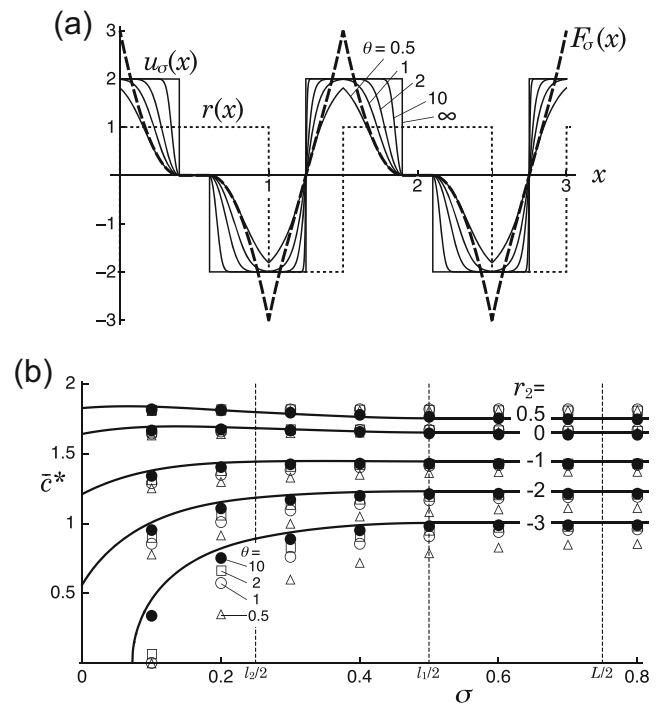


Fig. 4 A generalized taxis velocity function and the asymptotic speed. **a** A generalized taxis velocity is defined by $u_\sigma(x) = \hat{u} \tanh(\theta F_\sigma(x))$, where $r(x)$ is given by (11) and $F_\sigma(x)$ is given by Eq. 13c with the sensory acuity, $s(\xi) = 2/\sigma(1 - |\xi|/\sigma)$ for $0 \leq |\xi| < \sigma$ and 0 for $|\xi| \geq \sigma$. $F_\sigma(x)$ is illustrated by the *thick dashed line* for $\sigma = 0.4$, and $u_\sigma(x)$ is shown by *thin lines* for $\sigma = 0.4$ and $\theta = 1/2, 1, 2, 10$ and ∞ . $u_\sigma(x)$ for $\theta = \infty$ corresponds to the *solid line* in Fig. 1b. Other parameters are chosen as $\hat{u} = 2, r_1 = 1, r_2 = -2, l_1 = 1$, and $l_2 = 0.5$. **b** The asymptotic speeds numerically obtained for $\theta = 1/2, 1, 2$, and 10 are plotted by *triangles, open circles, squares, and closed circles*, respectively, on the same graph as in Fig. 2b. The *solid lines* represent the minimum TPW speeds c^* when $\theta = \infty$

the population becomes overcrowded in favorable patches while being extremely lowered in unfavorable patches, as seen in Fig. 3a (III). However, in the overpopulated area, animals would naturally tend to migrate to areas with a lower population density because of population pressure (see the “Introduction” section).

Here, we examine how non-linear diffusion caused by population pressure influences the spatio-temporal pattern of the asymptotic wave solution and its spreading speed. As mentioned in the “Introduction” section, we previously proposed a non-linear diffusion model for population pressure based on Morisita’s experiments using antlions (Shigesada et al. 1979). Incorporating that model into Eq. 13, we have the following non-linear reaction-diffusion-advection equation:

$$\frac{\partial n}{\partial t} = \frac{\partial^2}{\partial x^2} \{ (D_0 + \beta n)n \} - \frac{\partial u_\sigma(x)n}{\partial x} + (r(x) - \mu n)n. \quad (26)$$

The first term on the right-hand side of Eq. 26 represents a Fokker-Planck diffusion that describes random diffusion

based on local environmental information (Skellam 1973; Aronson 1985; Shigesada et al. 2015; Bengfort et al. 2016). $D_0 (\geq 0)$ is the diffusion constant in the absence of population pressure and βn represents the effect of population pressure on diffusivity meaning that random dispersal is more enhanced as the population density at the point of departure is higher. $\beta (\geq 0)$ is referred to as the population-pressure coefficient. For the intrinsic growth rate $r(x)$ and the taxis velocity $u_\sigma(x)$, we adopt a piecewise constant function (11) and the long-range taxis function defined by (13b, c), respectively. Since Theorem 1 is not applicable to Eq. 26 because of non-linearity in the diffusion term, we study (26) mostly by relying on computer simulations. To capture fundamental effects of population pressure, however, we first obtain the exact traveling wave solution of Eq. 26 for the specific case in which the environment is homogeneous, and then move to the full model for periodically patchy environments.

Effects of population pressure in a homogeneous environment

When the environment is homogeneous where $r_1 = r_2 = r$ and hence $u_\sigma(x) = 0$, Eq. 26 is reduced to

$$\frac{\partial n}{\partial t} = \frac{\partial^2}{\partial x^2} \{ (D_0 + \beta n)n \} + (r - \mu n)n. \tag{27}$$

Particularly, when $D_0 = 0$ and $\beta \neq 0$, Aronson (1980) and Newman (1980) showed that Eq. 27 has an explicit and exact traveling wave solution in the form,

$$n(z) = \begin{cases} \frac{r}{\mu} \left\{ 1 - \exp \left(\sqrt{\frac{\mu}{4\beta}} (z - z_c) \right) \right\} & (0 \leq z < z_c), \\ 0 & (z_c \leq z), \end{cases} \tag{28}$$

where $z = x - ct$, z_c is the front position of the wave at $t = 0$ and c is the speed of the traveling wave as given by

$$c = r \sqrt{\frac{\beta}{\mu}}. \tag{29}$$

Notably, the front of the wave at time t is given by $x = z_c + ct$, beyond which the population density is identically zero, thereby representing the so-called sharp-front wave (Sánchez-Garduño and Maini 1994). This frontal pattern fundamentally differs from the smooth-front wave that appears in the Fisher equation (Fisher 1937), i.e., Eq. 27 with $D_0 > 0$ and $\beta = 0$ (see Fig. 5b).

On the other hand, for the case in which both D_0 and β are positive, neither an explicit traveling wave solution

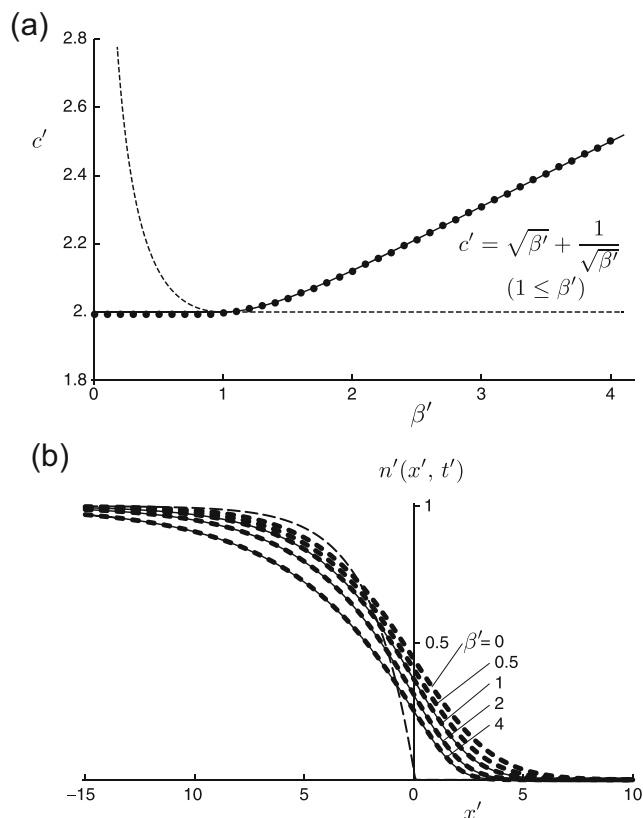


Fig. 5 Traveling wave solutions and their speeds of the non-linear reaction-diffusion equation in a homogeneous environment given by Eq. 31. **a** Mathematical formula for the minimum speed c' of the traveling wave, Eq. 32, is plotted as a function of the population pressure coefficient β' by a *thin line*, on which asymptotic wave speed \bar{c}' numerically obtained is superimposed by *black circles*. **b** Asymptotic solutions of Eq. 31 numerically calculated are illustrated for $\beta' = 0, 0.5, 1, 2,$ and 4 by *thick dashed lines*. Each solution is arranged in such a way that the inflection point of the solution falls on the vertical axis. Exact solutions of the traveling waves given by Eq. 33 are also illustrated by *thin solid lines* for $\beta' = 1, 2,$ and 4 . For each β' , the *thick dashed line* and *thin solid line* perfectly coincide with each other. For comparison, the traveling wave solution with a sharp-front as given by Eq. 28 for $r = \mu = \beta = 1$ is shown by the *thin dashed line*

nor its spreading speed seems to have been obtained so far. Thus, we investigate (27) both analytically and numerically, and find a formula for the minimum speed of traveling wave for any $\beta \geq 0$ and its explicit traveling wave solution for $\beta \geq 1$. The results are summarized below (see Appendix D for details). Let us introduce the following non-dimensional quantities:

$$n' = \frac{\mu}{r} n, \quad t' = rt, \quad x' = \sqrt{\frac{r}{D_0}} x, \quad \beta' = \frac{\beta r}{D_0 \mu}. \tag{30}$$

Then, Eq. 27 becomes

$$\frac{\partial n'}{\partial t'} = \frac{\partial^2}{\partial x'^2} \{ (1 + \beta' n')n' \} + (1 - n')n', \tag{31}$$

which contains only one parameter β' . We first carry out extensive computer simulations of Eq. 31 for various values of β' and confirm that any initial distributions with compact support asymptotically converge to a traveling wave with a smooth-front. We subsequently found that an exact formula for the minimum speed of traveling waves of Eq. 31 can be derived by using the theorem for the traveling wave solution obtained from a population genetic model by Haderler and Rothe (1975) and Haderler (1983) as shown below (see Appendix D for proof):

$$c' = \begin{cases} 2 & (0 \leq \beta' \leq 1), \\ \sqrt{\beta'} + \frac{1}{\sqrt{\beta'}} & (1 \leq \beta'). \end{cases} \tag{32}$$

It should be noted that the minimum speed for a given $\beta' > 0$ corresponds to the speed of the asymptotic propagating solution of Eq. 31 that starts with the initial data having compact support. We further find that, for any β' such that $\beta' \geq 1$, the exact and explicit traveling wave solution with the minimum speed c' is given as follows (see Appendix D):

$$\frac{(1 - n')^{2\beta'+1}}{n'} = e^{\sqrt{\beta'}(z-z_c)}, \tag{33}$$

where $z = x' - c't'$, $c' = \sqrt{\beta'} + 1/\sqrt{\beta'}$ and z_c is an arbitrary constant.

In Fig. 5a, the speed formula (32) is plotted as the thin line and the asymptotic speed \bar{c}' numerically obtained is indicated by closed circles. As expected, the speed numerically obtained closely fits the thin line. Interestingly, the speed remains at 2 independent of β' for $0 \leq \beta' \leq 1$ and then increases as β' increases above 1. In Fig. 5b, asymptotic solutions $n'(x', t')$ at a sufficiently large t' for $\beta' = 0, 0.5, 1, 2$, and 4 are illustrated by thick dashed curves. For convenience of comparison, the asymptotic solution for each β' is arranged in such a way that the inflection point of $n'(x', t')$, i.e., the point (x', n') at which $\partial^2 n' / \partial x'^2 = 0$, falls on the vertical axis. We can see that as β' increases, n' at the inflection point is reduced. The analytical traveling wave solution Eq. 33 for $\beta' = 1, 2$, and 4 is plotted by solid thin curves, which exactly fit with the corresponding simulated solutions for $\beta' = 1, 2$, and 4 (thick dashed curves). According to the classification by Stokes (1976), the fronts with minimum speed $c' = 2$ for $0 \leq \beta' \leq 1$ correspond to “pulled fronts” as their speed is determined by the leading edge of the traveling wave solution. On the other hand, the front with the minimum speed $c' = \sqrt{\beta'} + 1/\sqrt{\beta'}$ for $\beta' > 1$, which is larger than the minimum speed of pulled fronts, $c' = 2$, corresponds to a “pushed front” because the speed is determined not by the behavior of the leading edge

of the traveling wave, but by the whole wave-front (Rothe 1981; Garnier et al. 2012).

Now, by carrying out the reverse transformation of Eq. 32 using Eq. 30, we have the formula for the minimum speed of the traveling wave in the original dimension as

$$c = \begin{cases} 2\sqrt{rD_0} & (0 \leq \beta\hat{n} \leq D_0), \\ r\sqrt{\frac{\beta}{\mu}} + D_0\sqrt{\frac{\mu}{\beta}} & (D_0 \leq \beta\hat{n}), \end{cases} \tag{34}$$

where $\hat{n} = r/\mu$, which represents the carrying capacity of the logistic growth function. When $\beta \leq D_0/\hat{n}$, the speed is given by $c = 2\sqrt{rD_0}$, which is independent of β and exactly coincides with the traveling wave speed of the Fisher equation. Accordingly, when $\beta \leq D_0/\hat{n}$, the population pressure hardly influences the spreading speed. On the other hand, once β exceeds D_0/\hat{n} , the speed is monotonically increased as β increases. Particularly, when $D_0 = 0$ and $\beta > 0$, i.e., in the case of a degenerate non-linear diffusion, the speed is reduced to $r\sqrt{\beta/\mu}$, which of course is equal to the traveling wave speed given by Eq. 29.

Effects of population pressure in a periodic patchy environment

Now, we examine (26) for the case in which $D_0 > 0$ and $\beta \geq 0$ in periodic patchy environments. Carrying out numerical simulations of Eq. 26 for various sets of parameter values, we again confirm that, when the equilibrium state $n = 0$ of Eq. 26 is unstable, a population starting from any localized distribution evolves to an asymptotic wave that closely fits a traveling periodic wave defined by Eq. 8 in Theorem 1. Figure 6 illustrates the range expansion patterns when $\beta = 0$ and 1, respectively, while other parameters are fixed as $D_0 = 0.1$, $\hat{u} = 0.6$, $\sigma = 0.5$, $r_1 = 1$, $r_2 = -2$, $l_1 = 1$, $l_2 = 0.5$, and $\mu = 1$. Among these parameters, we put $D_0 = 0.1$ and $r_1 = \mu = 1$ without loss of generality, because they can be arbitrarily chosen by non-dimensionalizing (26). In Fig. 6a, where the population pressure does not work, the central areas of favorable patches are overcrowded to a level exceeding even the carrying capacity, $\hat{n} = 1$, whereas the unfavorable patches are underpopulated. On the other hand, in the presence of population pressure (Fig. 6b), the population density becomes drastically reduced in favorable patches, while significantly elevated in unfavorable patches. This means that the population pressure drives organisms from overcrowded areas in favorable patches to unfavorable patches, thereby making the distribution more uniform, as originally demonstrated in the Morisita’s experiment with antlions described in the “Introduction” section. As a consequence, it seems that the asymptotic

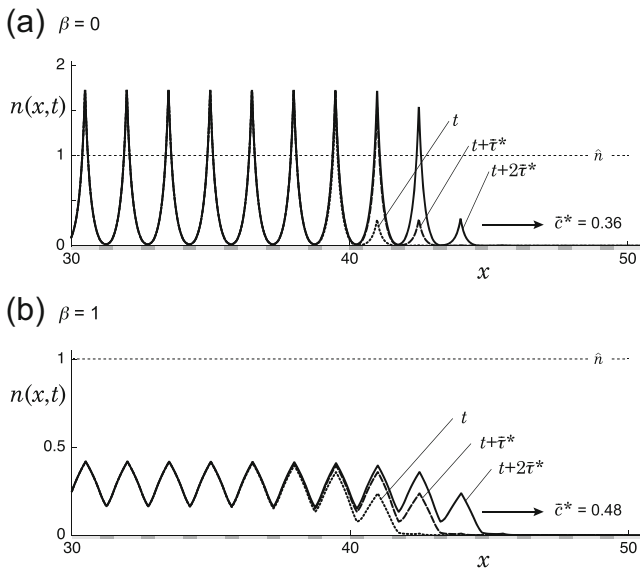


Fig. 6 Comparison of asymptotic solutions of Eq. 26 in the presence and absence of population pressure. Parameters are chosen as $\beta = 0$ in **a.** and $\beta = 1$ in **b.** Other parameters are fixed as $D_0 = 0.1$, $\sigma = 0.5$, $\hat{u} = 0.6$, $r_1 = 1$, $r_2 = -2$, $l_1 = 1$, $l_2 = 0.5$, and $\mu = 1$. The asymptotic solutions closely fit the definitions for the TPW defined by Eq. 8, where the values of t , $\bar{\tau}^*$ and $\bar{c}^* = L/\bar{\tau}^*$ are **a** 115.7, 4.13, and 0.36; and **b** 87.4, 3.12, and 0.48, respectively

spreading speed is accelerated. Incidentally, since (26) is rewritten as

$$\frac{\partial n}{\partial t} = D_0 \frac{\partial^2 n}{\partial x^2} - \frac{\partial}{\partial x} \left(u_\sigma(x)n - 2\beta \frac{\partial n}{\partial x} n \right) + (r(x) - \mu n)n, \tag{35}$$

the non-linear diffusion in Eq. 26 may be viewed as being equivalent to a simple random diffusion with an additional advection due to gradient-based taxis (short-range taxis) toward the direction of lower population density (Skellam 1951, 1973; Okubo and Levin 2001). In fact, we can see from Fig. 6b that $-2\beta \partial n / \partial x < 0$ where $u_\sigma(x) > 0$ and vice versa, so that the population pressure acts to attenuate the effect of the taxis velocity, $u_\sigma(x)$.

In Fig. 7a, the asymptotic speeds \bar{c}^* numerically calculated are plotted by closed circles linked by thin dashed straight lines as a function of taxis intensity \hat{u} for varying values of β . All curves exhibit one-humped shapes. The lowermost curve represents the speed without population pressure (i.e., $\beta = 0$). To be noted, the speed for $\beta = 0.1$ indistinguishably overlaps that for $\beta = 0$, but the speed for $\beta = 0.2$ slightly deviates from them. Thus, the asymptotic speed \bar{c}^* seems to be scarcely influenced by β when it is smaller than a certain value, at least for $0 < \beta < 0.1$ in the present case. As β is increased further, however, each curve shifts upwards while maintaining the one-humped shape.

This tendency is qualitatively consistent with the minimum traveling wave speed in a homogeneous environment

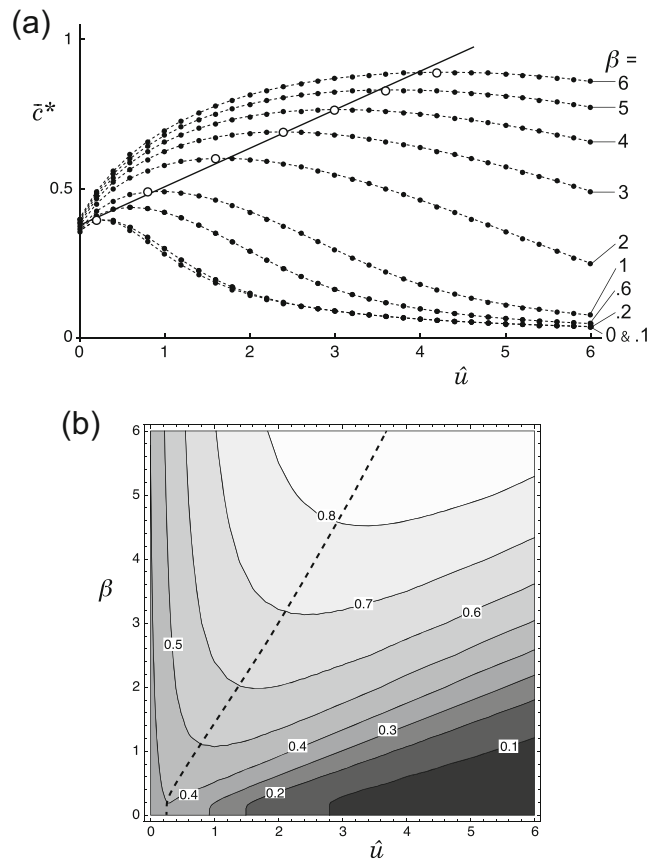


Fig. 7 a Asymptotic speed \bar{c}^* of the non-linear reaction-diffusion-advection Eq. 26 numerically obtained is plotted as a function of the taxis intensity \hat{u} for $\beta = 0, 0.1, 0.2, 0.6, 1, 2, \dots, 6$ by black circles linked with dashed straight lines. The other parameters are the same as in Fig. 6. The lowest curve indicates the asymptotic speed for $\beta = 0$ that is virtually indistinguishable from the asymptotic speed for $\beta = 0.1$. When β exceeds approximately 0.1, the speed monotonically increases with increases in β . The maximum speed for each value of β is indicated by an open circle. **b** A contour map of asymptotic speed \bar{c}^* on (\hat{u}, β) plane, where the other parameters are the same as in **a.** The boxed numerals indicate speed \bar{c}^* . The dashed line represents the ridge of contours

in which the speed maintains a constant value when β is smaller than a certain value and begins to increase as β further increases, as described in the “Effects of population pressure in a homogeneous environment” section.

The open circles in Fig. 7a indicate the maximum speed for each value of β . As β increases, the maximum speed is attained at larger values of \hat{u} . To better grasp the mutual influence of \hat{u} and β on the speed, we draw a contour map of the asymptotic speed \bar{c}^* on (\hat{u}, β) plane in Fig. 7b, where a lighter shade of gray indicates a higher speed. The dashed line indicates the ridge of the contour. To be noted, in the region for β smaller than around 0.1, the contours are all perpendicular to the x axis, which means that the speed is not influenced by β , as already pointed out in Fig. 7(a). From this figure, we can infer that the speed \bar{c}^* increases

most effectively when both \hat{u} and β are simultaneously increased along the ridge except for the region where β is close to zero. In other words, the population pressure and the taxis synergistically enhance the spreading speed.

Finally, we examine the effects of the scale of patch sizes by changing l_1 and l_2 . As representative examples, we consider two cases in which the patch size is doubled in l_2 only or in both l_1 and l_2 , relative to those adopted in Fig. 7 (i.e., $l_1 = 1, l_2 = 0.5$). In Fig. 8a, black circles for each β indicate the speed plotted against \hat{u} , when $(l_1, l_2) = (1, 1)$ with the other parameters fixed as $D_0 = 0.1, \sigma = 0.5, r_1 = 1, r_2 = -2$ and $\mu = 1$. For comparison, the corresponding results for $(l_1, l_2) = (1, 0.5)$ shown in Fig. 7a are superimposed in gray. As a matter of course, the speed is considerably reduced when the width of the unfavorable

patch alone is doubled. This tendency is more emphasized as both \hat{u} and β become larger. This finding seems reasonable, because larger unfavorable patches should cause greater reductions in population densities in both favorable and unfavorable patches with concomitant reductions in the synergistic effect of population pressure and taxis.

Likewise, in Fig. 8b, the speeds for $(l_1, l_2) = (2, 1)$ indicated by black circles are compared with the corresponding speeds for $(l_1, l_2) = (1, 0.5)$ shown by gray circles. Upon doubling both l_1 and l_2 , the speeds retain similar one-humped shapes. On closer examination, however, the point of the black circle at $\hat{u} = 0$ lies above that of the gray circle for each β . Namely, the speed is higher as the scale of the patch size is larger, as has been previously reported (Shigesada et al. 1986). On the other hand, the order of these speeds is reversed when \hat{u} exceeds a certain value for each β as indicated by double circles in Fig. 8b. Accordingly, the maximum point (open circle) for each β is shifted leftwards and slightly elevated compared with that of the corresponding gray curve. In other words, the maximum speed is attained at a smaller value of taxis intensity \hat{u} for each β . This means that the effect of taxis is enhanced by enlargement of the patch scale (see also Kawasaki et al. 2012).

Discussion

We have presented a new model for biological invasions in periodic patchy environments, in which long-range taxis and population pressure are incorporated in the framework of reaction-diffusion-advection equations. We assumed that long-range taxis is induced by a weighted integral of stimuli from the environment. As the simplest case, we employed the taxis velocity function given by Eq. 13b, which is specified by two parameters, the sensing length σ and the taxis intensity \hat{u} . The population pressure is incorporated into the diffusion coefficient that linearly increases with population density.

We first analyzed the model in the absence of population pressure and demonstrated how long-range taxis influences the asymptotic solution that starts with a localized distribution and its spreading speed. The effects of population pressure were then examined for both homogeneous and periodic patchy environments. The main results are as follows. In the absence of population pressure, (i) any solution evolves to a unique asymptotic wave or tends to zero depending on whether the equilibrium state $n = 0$ is unstable or stable, respectively; (ii) with increases in the taxis intensity \hat{u} , the minimum TPW speed c^* shows a one-humped curve that tends to zero as $\hat{u} \rightarrow \infty$; (iii) with increases in the sensing length σ , the minimum TPW speed c^* initially increases but tends to become saturated

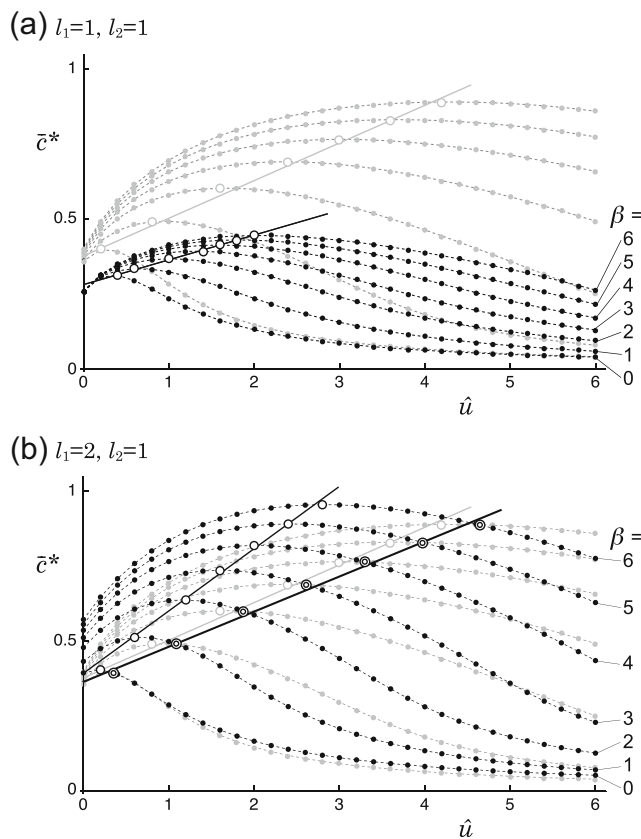


Fig. 8 Asymptotic speed \bar{c}^* of the non-linear reaction-diffusion-advection equation (26) as a function of taxis intensity \hat{u} for $\beta = 0, 1, 2, \dots, 6$. **a** Black circles represent the asymptotic speed when $(l_1, l_2) = (1, 1)$ with the other parameters kept the same as in Fig. 6. The maximum speed for each β is indicated by an open circle. The asymptotic speeds in the case of $(l_1, l_2) = (1, 0.5)$ as shown in Fig. 7a are superimposed by gray circles for comparison. **b** Black circles represent the asymptotic speed when $(l_1, l_2) = (2, 1)$ with the other parameters kept the same as in **a**. The maximum speed for each β is indicated by an open circle. The asymptotic speeds for $(l_1, l_2) = (1, 0.5)$ are superimposed in gray as in **a**. The double circles represent the points at which the asymptotic speeds for $(l_1, l_2) = (2, 1)$ and $(1, 0.5)$ cross each other

after σ exceeds $\max(l_1/2, l_2/2)$. In the presence of population pressure, (iv) traveling wave solutions in homogeneous environments and their speeds can be analytically obtained; (v) in periodic environments, population pressure acts to monotonically increase the asymptotic speed c^* . Furthermore, the speed is synergistically enhanced by population pressure and taxis intensity when they are both increased in a positively correlated manner.

As described in the “[Previous work — existence of asymptotic spreading speeds and traveling periodic waves](#)” section, we have recently investigated a reaction-diffusion-advection Eq. 7 that incorporates short-range taxis with the taxis velocity of $u(x) = \alpha dr(x)/dx$ (Shigesada et al. 2015). Since $r(x)$ is piecewise constant, taxis occurs only at the interfaces between the favorable and unfavorable patches with infinitely large taxis velocities. More specifically, $u(x) = \alpha(r_1 - r_2)\delta(x)$ where $\delta(x)$ is the Dirac delta function. By solving this model both numerically and analytically, we found that if the equilibrium state $n = 0$ is unstable, any solution evolves to a unique asymptotic wave in which the population density discontinuously jumps at the interfaces, but remains nearly flat within each patch (Shigesada et al. 2015; see also Maciel and Lutscher 2013). This flattened distribution in each patch with discontinuous jumps at the boundaries between neighboring patches is in marked contrast with the continuous but sharply aggregated distribution within each favorable patch as observed in the long-range taxis model (see Fig. 2a (III)). Nevertheless, the effect of taxis intensity \hat{u} on the TPW speed in the long-range taxis model qualitatively resembles the effect of the taxis sensitivity α in the short-range taxis model in that both exhibit one-humped response curves (Kawasaki et al. 2012; Shigesada et al. 2015).

In the integral-based long-range taxis model, we have implicitly assumed that the taxis velocity, as defined by Eqs. 3a and 4a, is density independent. There have been a few integral-based long-range taxis models that include density-dependent effects mostly focusing on animal or cell aggregation. For example, Kawasaki (1978) (see also Turchin 1998) proposed a model for animal aggregation, in which taxis is induced by the difference between the total populations in the habitats on the left and right sides, and Armstrong et al. (2006) explained the aggregation of adhesive cells in both 1- and 2-dimensions using a sophisticated density-dependent integral-based taxis model that they referred to as a non-local taxis model. However, the range expansion in heterogeneous environments was beyond the scope of their studies.

In the “[Effects of population pressure in a homogeneous environment](#)” section, we have examined a Fisher equation with non-linear diffusion for a homogeneous environment as given by Eq. 27 and derived the traveling wave solution and its speed in an explicit forms. There have been

several other candidates for non-linear diffusion that incorporate population pressure. For convenience of comparison, let us consider a Fisher equation with non-linear diffusion of Fickian type as follows (Okubo and Levin 2001):

$$\frac{\partial n}{\partial t} = \frac{\partial}{\partial x} \left(D(n) \frac{\partial n}{\partial x} \right) + (1 - n)n. \quad (36)$$

When $D(n) = D_0 + 2\beta n$, the above equation is equivalent to Eq. 27. Shakeel (2013) investigated (36) for $D(n) = D_m e^{\gamma(n-1)}$ ($D_m > 0$, $\gamma \geq 0$, $0 \leq n \leq 1$) and numerically found that when γ is smaller than a certain value, the spreading speed of the asymptotic wave remains constant, whereas the speed starts to increase as γ exceeds that threshold. This result is qualitatively similar to the characteristic properties found in the minimum traveling wave speed as given by Eq. 32. Furthermore, in the two cases above where the values of $D(0)$ are not zero, the traveling wave solutions form a smooth-front wave. On the other hand, when the diffusion term is degenerate, i.e., $D(0) = 0$ with $D(n) > 0$ for $n \in (0, 1]$, Sánchez-Garduño and Maini (1994) proved the existence and uniqueness of a sharp-front traveling wave for a large family of Fisher equations. However, as for the Fisher equation with non-linear diffusion in a periodic patchy environment, the existence of a traveling periodic wave and its rate of spread have mathematically not yet been proven for either non-degenerate or degenerate non-linear diffusion. Although the simulation results presented in the “[Effects of population pressure in a periodic patchy environment](#)” are based on the simplest non-linear diffusion model for a heterogeneous environment, we hope that they may provide a basis for understanding how population pressure, long-range taxis and spatial heterogeneity of environment interplay to influence the spatial pattern and its rate of spread.

Acknowledgments We would like to acknowledge our special thanks to H. F. Weinberger for his valuable discussion and helpful suggestions. We also thank O. Diekmann for his informative comments and two referees for useful suggestions. This work is partly supported by Grant-in-Aid for Scientific Research on Innovation Areas from the Japan Ministry of Education, Science, Culture and Sports 22101004 to KK.

Open Access This article is distributed under the terms of the Creative Commons Attribution 4.0 International License (<http://creativecommons.org/licenses/by/4.0/>), which permits unrestricted use, distribution, and reproduction in any medium, provided you give appropriate credit to the original author(s) and the source, provide a link to the Creative Commons license, and indicate if changes were made.

Appendix A: Derivation of Eq. 14

Since $s(\xi) = s(-\xi)$, $F_\sigma(x)$ is rewritten in the following form:

$$F_\sigma(x) = \int_0^\sigma s(\xi)R_x(\xi)d\xi, \tag{37}$$

where

$$R_x(\xi) = r(x + \xi) - r(x - \xi), \tag{38}$$

and the value of $R_x(\xi)$ at discontinuity points is assumed to be zero.

As mentioned in the “Taxis velocity” section, $r(x)$ has the following properties:

$$r(x) = r(x + L) \quad (L\text{-periodic in } x), \tag{39a}$$

$$r(x) = r(l_1/2 - x) \quad (\text{even with respect to } x = L/2). \tag{39b}$$

Using Eq. 39a, we have

$$R_x(\xi) = R_x(\xi + L) \quad (L\text{-periodic in } \xi), \tag{40a}$$

$$R_x(\xi) = -R_x(L - \xi) \quad (\text{odd with respect to } \xi = L/2). \tag{40b}$$

Thus, if we know $R_x(\xi)$ for $0 \leq \xi \leq L/2$, $R_x(\xi)$ can be extrapolated for $0 \leq \xi \leq L$. Furthermore, by using Eq. 39, we have

$$R_x(\xi) = R_{x+L}(\xi) \quad (L\text{-periodic in } x), \tag{41a}$$

$$R_x(\xi) = -R_{l_1-x}(\xi) = -R_{2l_1+l_2-x}(\xi) \tag{41b}$$

(odd with respect to $x = l_1/2$ and $l_1 + l_2/2$).

Combining (40) and (41) yields that if we know $R_x(\xi)$ for $0 \leq x \leq l_1/2$ and $l_1 \leq x \leq l_1 + l_2/2$, $R_x(\xi)$ can be extrapolated for $0 \leq x \leq L$.

Now substituting (41a) into (37), we obtain $F_\sigma(x) = F_\sigma(x + L)$. Thus, Eq. 14a is proved. Similarly, applying $R_x(\xi) = -R_{l_1-x}(\xi)$ in Eq. 41b to Eq. 37, we have $F_\sigma(x) = -F_\sigma(l_1 - x)$. Thus, Eq. 14b is proved.

Appendix B: Derivation of (16)

We first calculate $R_x(\xi)$ for $0 \leq \xi \leq L/2$ when x is a point in $0 \leq x \leq l_1/2$ or $l_1 \leq x \leq l_1 + l_2/2$. From the definition (38), we have

(a) when $0 \leq x \leq l_1/2$,

$$R_x(\xi) = \begin{cases} 0 & (0 \leq \xi \leq x), \\ r_1 - r_2 & (x < \xi < \min(l_1 - x, L - (l_1 - x))), \\ 0 & (\min(l_1 - x, L - (l_1 - x)) \leq \xi \leq L/2), \end{cases} \tag{42}$$

(b) when $l_1 \leq x \leq l_1 + l_2/2$,

$$R_x(\xi) = \begin{cases} 0 & (0 \leq \xi \leq x - l_1), \\ -(r_1 - r_2) & (x - l_1 < \xi < \min(x, L - x)), \\ 0 & (\min(x, L - x) \leq \xi \leq L/2), \end{cases} \tag{43}$$

Using Eqs. 40 and 41, Eqs. 42 and 43 are extrapolated to $R_x(\xi)$ for $0 \leq \xi \leq L$ and $0 \leq x \leq L$ as follows:

$$R_x(\xi) = \begin{cases} 0 & (0 \leq \xi \leq x_1), \\ R_{12} & (x_1 < \xi < x_2), \\ 0 & (x_2 \leq \xi \leq L - x_2), \\ -R_{12} & (L - x_2 < \xi < L - x_1), \\ 0 & (L - x_1 \leq \xi \leq L), \end{cases} \tag{44}$$

where

(1) when $0 \leq x < l_1/2$,

$$R_{12} = r_1 - r_2 > 0, \quad x_1 = x \quad \text{and} \\ x_2 = \min(l_1 - x, L - (l_1 - x)),$$

(2) when $l_1/2 \leq x < l_1 + l_2/2$,

$$R_{12} = -r_1 + r_2 < 0, \quad x_1 = |l_1 - x| \quad \text{and} \\ x_2 = \min(x, L - x),$$

(3) when $l_1 + l_2/2 \leq x < L$,

$$R_{12} = r_1 - r_2 > 0, \quad x_1 = x \quad \text{and} \\ x_2 = \min(x - l_1, L - (x - l_1)).$$

The above results indicate that $R_x(\xi)$ is odd with respect to $\xi = L/2$ as shown in Eq. 40b, and that $R_x(\xi) \geq 0$ for $0 \leq \xi < L/2$ when $0 \leq x < l_1/2$ or $l_1 + l_2/2 \leq x < L$, and $R_x(\xi) \leq 0$ for $0 \leq \xi < L/2$ when $l_1/2 \leq x < L - l_2/2$. Taking these results into account together with the condition for $s(\xi)$ in Eq. 12b, the sign of $F_\sigma(x)$ is given as follows:

$$F_\sigma(x) = \int_0^\sigma s(\xi)R_x(\xi)d\xi = \begin{cases} + & (0 \leq \xi < \sigma_1), \\ 0 & (\sigma_1 \leq \xi \leq l_1 - \sigma_1), \\ - & (l_1 - \sigma_1 < \xi < l_1 + \sigma_2), \\ 0 & (l_1 + \sigma_2 \leq \xi \leq L - \sigma_2), \\ + & (L - \sigma_2 < \xi \leq L), \end{cases} \tag{45}$$

where $\sigma_1 = \min(\sigma, l_1/2)$ and $\sigma_2 = \min(\sigma, l_2/2)$.

Applying Eq. 45 to Eq. 13b, we obtain (16) in the text.

Appendix C: Derivation of Eq. 24 and criterion for successful invasion

Derivation of Eq. 24

Because $A^{(0,L)}$ is a 2×2 matrix, Eq. 23 is rewritten as

$$(e^{-sL})^2 - \text{tr} A^{(0,L)}e^{-sL} + \det A^{(0,L)} = 0. \tag{46}$$

Since the determinant of each $A_{(u,r)}^{(a,b)}$ in Eq. 22c is $e^{\frac{u(b-a)}{2D}}$, we have $\det A^{(0,L)} = 1$. Thus, Eq. 46 is reduced to

$$\text{tr} A^{(0,L)} = e^{sL} + e^{-sL} = 2 \cosh(sL), \tag{47}$$

which leads to Eq. 24 in the text.

Criterion for successful invasion

As described in Theorem 1, the criterion for successful invasion is given by the condition that the trivial solution $n = 0$ of Eq. 13 is unstable. Thus, we consider the linearized Eq. 17 and obtain the condition under which the principal eigenvalue of the following equation is positive:

$$D \frac{d^2 n}{dx^2} - \frac{du(x)n}{dx} + (r(x) - \Lambda)n = 0, \tag{48}$$

where Λ is the eigenvalue. Incidentally, the characteristic equation of (48) is given by Eq. 23 in which s and λ are set 0 and $r(x)$ is replaced by $r(x) - \Lambda$, or equivalently s is set 0 and λ is replaced by Λ . Thus, the condition for the eigenvalue of Eq. 48 to be zero, i.e., $\Lambda = 0$, is given by Eq. 47 with $s = \lambda = 0$:

$$\text{tr}A^{(0,L)}|_{\lambda=0} = 2,$$

which indicates the boundary separating stable and unstable regions in the parameter space. We numerically find that the parameter region in which the primary eigenvalue of $\text{tr}A^{(0,L)} = 2$ is positive is given by

$$\text{tr}A^{(0,L)}|_{\lambda=0} < 2.$$

Appendix D: The minimum speed and the exact solution of the traveling wave of Eq. 31

Consider

$$\frac{\partial n}{\partial t} = \frac{\partial}{\partial x} \left(D(n) \frac{\partial n}{\partial x} \right) + F(n), \tag{49}$$

where

$$F(0) = F(1) = 0, F(n) > 0 \ (0 < n < 1), \\ D(n) > 0 \ (n \geq 0), F(n) \text{ and } D(n) \in C^1.$$

A traveling wave of Eq. 49 with speed $c \geq 0$ is a solution of the form

$$n(x, t) = u(z), \ z = x - ct, \tag{50}$$

which is subject to the following conditions:

$$\lim_{z \rightarrow -\infty} u(z) = 1, \ \lim_{z \rightarrow \infty} u(z) = 0 \text{ and } 0 \leq u(z) \leq 1.$$

Substituting (50) into (49) and setting $u' = v$, where the prime denotes differentiation with respect to z , we have the following set of ODEs:

$$u' = v, \tag{51a}$$

$$v' = \frac{-cv - D'(u)v^2 - F(u)}{D(u)}, \tag{51b}$$

which are subject to

$$\lim_{z \rightarrow -\infty} u(z) = 1, \ \lim_{z \rightarrow \infty} u(z) = 0, \\ \lim_{z \rightarrow -\infty} v(z) = \lim_{z \rightarrow \infty} v(z) = 0 \text{ and } 0 \leq u(z) \leq 1. \tag{52}$$

Hadeler and Rothe (1975) and Hadeler (1983) presented seminal work on traveling waves of Eq. 49, of which the part relevant to Eq. 31 is summarized as follows:

(I) Hadeler (1983) showed that with the following variable transformations,

$$\tilde{u} = u, \ \tilde{v} = D(u)v, \ \tilde{z} = \int_0^z \frac{ds}{D(s)}, \ \tilde{F}(\tilde{u}) = F(\tilde{u})D(\tilde{u}), \tag{53}$$

Equation 51 is transformed to

$$\tilde{u}' = \tilde{v}, \\ \tilde{v}' = -c\tilde{v} - \tilde{F}(\tilde{u}), \tag{54}$$

which are subject to

$$\lim_{\tilde{z} \rightarrow -\infty} \tilde{u}(\tilde{z}) = 1, \ \lim_{\tilde{z} \rightarrow \infty} \tilde{u}(\tilde{z}) = 0, \\ \lim_{\tilde{z} \rightarrow -\infty} \tilde{v}(\tilde{z}) = \lim_{\tilde{z} \rightarrow \infty} \tilde{v}(\tilde{z}) = 0 \text{ and } \tilde{u}(\tilde{z}) \geq 0$$

(see also Engler 1985 and Gilding and Kersner 2004).

(II) Hadeler and Rothe (1975) showed that when

$$\tilde{F}(\tilde{u}) = \tilde{u}(1 - \tilde{u})(1 + 2\beta\tilde{u}), \tag{55}$$

there exist traveling waves of Eq. 54 for $\beta \geq -1/2$ and the minimum speed for each β is given as

$$c^* = \begin{cases} 2 & (-\frac{1}{2} < \beta \leq 1), \\ \sqrt{\beta} + \frac{1}{\sqrt{\beta}} & (1 \leq \beta). \end{cases} \tag{56}$$

Furthermore, when $\beta \geq 1$, the explicit traveling wave solution with the minimum speed c^* is given as

$$\tilde{u}(\tilde{z}) = \frac{1}{1 + e^{\sqrt{\beta}\tilde{z}}}. \tag{57}$$

Now let us consider (49) with $D(u) = 1 + 2\beta u$ and $F(u) = u(1 - u)$, which is equivalent to Eq. 31. By applying the transformation (53) to (51) with $D(u) = 1 + 2\beta u$ and $F(u) = u(1 - u)$, we have Eq. 54 with $\tilde{F}(\tilde{u}) = \tilde{u}(1 - \tilde{u})(1 + 2\beta\tilde{u})$, which is exactly the same as Eq. 55. Therefore the minimum speed of the traveling wave of Eq. 49 for $D(n) = 1 + 2\beta n$ and $F(n) = n(1 - n)$ is given by Eq. 56.

To obtain the traveling wave solution of Eq. 31 corresponding to Eq. 57, we need to carry out a reverse transformation of Eq. 57 by using Eq. 53 as follows:

From Eqs. 53, 54 and 57, we have

$$D(u)v = \tilde{v} = \tilde{u}'(\tilde{z}) = -\frac{\sqrt{\beta}e^{\sqrt{\beta}\tilde{z}}}{(1 + e^{\sqrt{\beta}\tilde{z}})^2} \quad (58)$$

$$= -\sqrt{\beta}(1 - \tilde{u})\tilde{u} = -\sqrt{\beta}(1 - u)u.$$

Using $u' = v$ and the above equation, we have

$$u' = -\frac{\sqrt{\beta}(1 - u)u}{D(u)} = -\frac{\sqrt{\beta}(1 - u)u}{1 + 2\beta u}. \quad (59)$$

Solving Eq. 59 gives

$$\frac{(1 - u)^{2\beta+1}}{u} = e^{\sqrt{\beta}(z - z_c)}.$$

Thus, Eq. 33 is proved.

References

- Armstrong NJ, Painter KJ, Sherratt JA (2006) A continuum approach to modelling cell-cell adhesion. *J Theor Biol* 243:98–113
- Aronson DG (1980) Density-dependent interaction-diffusion systems. In: Stewart WE, Ray WH, Conley CC (eds) *Dynamics and Modelling of Reactive Systems*. Academic Press, New York, pp 161–176
- Aronson DG (1985) The role of diffusion in mathematical population biology: Skellam revisited. In: Capasso V, Grosso E, Pavri-Fontana SL (eds) *Mathematics in Biology and Medicine*. Lecture Notes in Biomathematics, vol 57, pp 2–6
- Bengfort M, Malchow H, Hilker FM (2016) The Fokker-Planck law of diffusion and pattern formation in heterogeneous media. *J Math Biol* 73:683–704
- Berestycki H, Hamel F, Roques L (2005a) Analysis of the periodically fragmented environment model: I - Species persistence. *J Math Biol* 51:75–113
- Berestycki H, Hamel F, Roques L (2005b) Analysis of the periodically fragmented environment model: II biological invasions and pulsating travelling fronts. *J Math Pures Appl* 84:1101–1146
- Cantrell RS, Cosner C, Lou Y (2006) Movement toward better environments and the evolution of rapid diffusion. *Math Biosci* 204:199–214
- Chesson P (2000) General theory of competitive coexistence in spatially-varying environments. *Theor Popul Biol* 58:211–237
- Dewhurst D, Lutscher F (2009) Dispersal in heterogeneous habitats: thresholds, spatial scales, and approximate rates of spread. *Ecology* 90:1338–1345
- Engler H (1985) Relations between travelling wave solutions of quasi-linear parabolic equations. *Proc Am Math Soc* 93:297–302
- Fisher RA (1937) The wave of advance of advantageous genes. *Ann Eugenics* 7:255–369
- Garnier J, Giletti T, Hamel F, Roques L (2012) Inside dynamics of pulled and pushed fronts. *J Math Pures Appl* 98:428–449
- Gilbert MA, White SM, Bullock JM, Gaffney EA (2014) Spreading speeds for stage structured plant populations in fragmented landscapes. *J Theor Biol* 349:135–149
- Gilding BH, Kersner R (2004) *Travelling waves in nonlinear diffusion-convection reaction*. Progress in nonlinear differential equations and their applications, vol 60. Basel, Birkhäuser Verlag
- Gurney WSC, Nisbet RM (1975) The regulation of inhomogeneous populations. *J Theor Biol* 52:441–457
- Gurtin ME, MacCamy RC (1977) On the diffusion of biological populations. *Math Biosci* 33:35–49
- Hadeler KP (1983) Free boundary problems in biological models. In: Fasano A, Primicerio M (eds) *Free Boundary Problems: Theory and Applications*, Vol II. Pitman, London, pp 665–671
- Hadeler KP, Rothe F (1975) Travelling fronts in non-linear diffusion equations. *J Math Biol* 2:251–263
- Hastings A, Cuddington K, Davies KF, Dugaw CJ, Elmendorf S, Freestone A, Harrison S, Holland M, Lambrinos J, Malvadkar U, Melbourne BA, Moore K, Taylor C, Thomson D (2005) The spatial spread of invasions: new developments in theory and evidence. *Ecol Lett* 8:91–101
- Hillen T, Painter KJ (2009) A user's guide to PDE models for chemotaxis. *J Math Biol* 58:183–217
- Kawasaki K (1978) Diffusion and the formation of spatial distribution. *Mater Sci* 183:47–52. (in Japanese)
- Kawasaki K, Shigesada N (2007) An integrodifference model for biological invasions in a periodically fragmented environment. *J pan J Indust Appl Math* 24:3–15
- Kawasaki K, Asano K, Shigesada N (2012) Impact of directed movement on invasive spread in periodic patchy environments. *Bull Math Biol* 74:1448–1467
- Keller EF, Segel LA (1970) Initiation of slime mold aggregation viewed as an instability. *J Theor Biol* 26:399–415
- Kinezaki N, Kawasaki K, Shigesada N (2010) The effect of the spatial configuration of habitat fragmentation on invasive spread. *Theor Popul Biol* 78:298–308
- Kinezaki N, Kawasaki K, Takasu F, Shigesada N (2003) Modeling biological invasions into periodically fragmented environments. *Theor Popul Biol* 64:291–302
- Kono T (1952) Time-dispersion curve: experimental studies on the dispersion of insects, 2. *Res Popul Ecol* 1:109–118. Japanese with English summary
- Lewis MA, Petrovskii SV, Potts JR (2016) *The mathematics behind biological invasions*. Springer
- Li B, Fagan WF, Meyer KI (2015) Success, failure, and spreading speeds for invasions on spatial gradients. *J Math Biol* 70:265–287
- Lutscher F (2008) Density-dependent dispersal in integrodifference equations. *J Math Biol* 56:499–524
- Lutscher F, Lewis MA, McCauley E (2006) Effects of heterogeneity on spread and persistence in rivers. *Bull Math Biol* 68:2129–2160
- Maciel GA, Lutscher F (2013) How individual movement response to habitat edges affects population persistence and spatial spread. *Am Nat* 182:42–52
- Maciel GA, Lutscher F (2015) Allee effects and population spread in patchy landscapes. *J Biol Dynamics* 9:109–123
- Mimura M, Kawasaki K (1980) Spatial segregation in competitive interaction-diffusion equations. *J Math Biol* 9:49–64
- Mistro DC, Rodrigues LAD, Ferreira Jr. WC (2005) The Africanized honey bee dispersal: a mathematical zoom. *Bull Math Biol* 67:281–312
- Morisita M (1954) Dispersion and population pressure: experimental studies on the population density of an ant-lion, *Glenuroides japonicus* M'L (II). *Japanese J Ecol* 4:71–79. Japanese with English summary
- Morisita M (1971) Measuring of habitat value by the “environmental density” methods. In: Patil GP, Pielou EC, Waters WE (eds) *Statistical Ecology*, vol 1. Penn. State Univ. Press, University Park, PA, pp 379–401
- Musgrave J, Lutscher F (2014) Integrodifference equations in patchy landscapes II: Population level consequences. *J Math Biol* 69:617–658
- Musgrave J, Girard A, Lutscher F (2015) Population spread in patchy landscapes under a strong Allee effect. *Theor Ecol* 8:313–326
- Myers JH, Krebs CJ (1974) Population cycles in rodents. *Sci Am* 230:38–46

- Namba T (1980) Density-dependent dispersal and spatial distribution of a population. *J Theor Biol* 86:351–363
- Newman WI (1980) Some exact solutions to a nonlinear diffusion problem in population genetics and combustion. *J Theor Biol* 85:325–334
- Okubo A, Levin SA (2001) *Diffusion and ecological problems: modern perspectives*. Springer, New York
- Othmer HG, Hillen T (2002) The diffusion limit of transport equations II: chemotaxis equations. *SIAM J Appl Math* 62:1222–1250
- Roques L, Stolica R (2007) Species persistence decreases with habitat fragmentation: an analysis in periodic stochastic environments. *J Math Biol* 55:189–205
- Rothe F (1981) Convergence to pushed fronts. *Rocky Mountain J Math* 11:617–634
- Samia Y, Lutscher F (2010) Coexistence and spread of competitors in heterogeneous landscapes. *Bull Math Biol* 72:2089–2112
- Sánchez-Garduño F, Maini PK (1994) Existence and uniqueness of a sharp travelling wave in degenerate non-linear diffusion Fisher-KPP equations. *J Math Biol* 33:163–192
- Shakeel M (2013) Travelling wave solution of the Fisher-Kolmogorov equation with non-linear diffusion. *Appl Math* 4:148–160
- Shigesada N (1980) Spatial distribution of dispersing animals. *J Math Biol* 9:85–96
- Shigesada N, Kawasaki K (1997) *Biological invasions: theory and practice*. Oxford Univ. Press, Oxford
- Shigesada N, Roughgarden J (1982) The role of rapid dispersal in the population dynamics of competition. *Theor Popul Biol* 21:353–372
- Shigesada N, Kawasaki K, Teramoto E (1979) Spatial segregation of interacting species. *J Theor Biol* 79:83–99
- Shigesada N, Kawasaki K, Teramoto E (1986) Traveling periodic waves in heterogeneous environments. *Theor Popul Biol* 30:143–160
- Shigesada N, Kawasaki K, Weinberger HF (2015) Spreading speeds of invasive species in a periodic patchy environment: effects of dispersal based on local information and gradient-based taxis. *J Pan J Indust Appl Math* 32:675–705
- Skellam JG (1951) Random dispersal in theoretical populations. *Biometrika* 38:196–218
- Skellam JG (1973) The formulation and interpretation of mathematical models of diffusionary processes in population biology. In: Bartlett MS, Hiorns RW (eds) *The Mathematical Theory of the Dynamics of Biological Populations*. Academic Press, New York, pp 63–85
- Stokes AN (1976) On two types of moving front in quasilinear diffusion. *Math Biosci* 31:307–315
- Turchin P (1998) *Quantitative analysis of movement: measuring and modeling population redistribution in animals and plants*. Sinauer, Sunderland, MA
- Vergni D, Iannaccone S, Berti S, Cencini M (2012) Invasions in heterogeneous habitats in the presence of advection. *J Theor Biol* 301:141–152
- Watanabe S, Utida S, Yosida T (1952) Dispersion of insect and change of distribution type in its process: experimental studies on the dispersion of insects, 1. *Res Popul Ecol* 1:94–108. Japanese with English summary
- Weinberger HF (2002) On spreading speeds and traveling waves for growth and migration models in a periodic habitat. *J Math Biol* 45:511–548
- Weinberger HF, Kawasaki K, Shigesada N (2008) Spreading speeds of spatially periodic integro-difference models for populations with nonmonotone recruitment functions. *J Math Biol* 57:387–411
- White KAJ, Lewis MA, Murray JD (1996) A model for wolf-pack territory formation and maintenance. *J Theor Biol* 178:29–43